© 2022. Published by The Company of Biologists Ltd | Journal of Cell Science (2022) 135, jcs259092. doi:10.1242/jcs.259092

RESEARCH ARTICLE

Recruitment of Peroxin 14 to lipid droplets affects lipid storage in *Drosophila*

Kazuki Ueda[1,*], Matthew N. Anderson-Baron[1,2,*], Julie Haskins[1], Sarah C. Hughes[1,3] and Andrew J. Simmonds[1,‡]

ABSTRACT

Both peroxisomes and lipid droplets regulate cellular lipid homeostasis. Direct inter-organellar contacts as well as novel roles for proteins associated with peroxisome or lipid droplets occur when cells are induced to liberate fatty acids from lipid droplets. We have shown a non-canonical role for a subset of peroxisome-assembly [Peroxin (Pex)] proteins in this process in *Drosophila*. Transmembrane proteins Pex3, Pex13 and Pex14 were observed to surround newly formed lipid droplets. Trafficking of Pex14 to lipid droplets was enhanced by loss of Pex19, which directs insertion of transmembrane proteins like Pex14 into the peroxisome bilayer membrane. Accumulation of Pex14 around lipid droplets did not induce changes to peroxisome size or number, and co-recruitment of the remaining Peroxins was not needed to assemble peroxisomes observed. Increasing the relative level of Pex14 surrounding lipid droplets affected the recruitment of Hsl lipase. Fat body-specific reduction of these lipid droplet-associated Peroxins caused a unique effect on larval fat body development and affected their survival on lipid-enriched or minimal diets. This revealed a heretofore unknown function for a subset of Pex proteins in regulating lipid storage.

This article has an associated First Person interview with Kazuki Ueda, joint first author of the paper.

KEY WORDS: *Drosophila*, Lipid droplets, Perilipins, Peroxins

INTRODUCTION

Peroxisomes are responsible for catabolism of very-long-chain fatty acids (VLCFAs) and branched chain fatty acids, biosynthesis of ether lipids and regulation of reactive oxygen (He et al., 2021). They are composed of a membrane bilayer with peroxisome membrane proteins (PMPs), surrounding a dense core of enzymes (Fujiki et al., 2020). Peroxisome number, size and enzyme composition change dynamically in response to demand (Honsho et al., 2016). New peroxisomes arise via fission of existing organelles but can be assembled *de novo*. Either process requires new membrane supplied as pre-peroxisomal vesicles (PPVs) into which PMPs are inserted (Fujiki et al., 2020). The peroxisome assembly process requires the coordinated activity of ten uniquely numbered Peroxin (Pex) proteins that are highly conserved in eukaryotes, as well as Pex11, which directs fission of existing peroxisomes (Fujiki et al., 2020). In animal cells, PPV budding from the endoplasmic reticulum (ER) requires Pex3 and Pex16 (Fakieh et al., 2013; Geuze et al., 2003; van der Zand et al., 2010; van der Zand and Tabak, 2013). Mitochondrial-derived PPVs are also thought to form in a Pex3-dependent manner (Kim, 2017; Rucktaschel et al., 2010; Sugiura et al., 2017). Pex19 recruits PMPs from the cytosol, directing them to membranes in a Pex3 (Type I)- or Pex3/Pex16 (Type II)-dependent process (Fujiki et al., 2020). Together, PMPs Pex13 and Pex14 form a transmembrane (TM) pore (docking complex) through which enzymes with a peroxisome-targeting sequence 1 (PTS1, SKL) motif are recruited from the cytoplasm Pex5 binding Pex14 in the docking complex. Pex5 is subsequently cycled out of the peroxisome by the Pex2, Pex10 and Pex12 E3 ligase complex and AAA-ATPase proteins Pex1 and Pex6 (Fujiki et al., 2020). Defects in any step of this process due to Pex gene mutations cause peroxisome biogenesis disorders like the Zellweger spectrum disorders (Fujiki et al., 2020).

Lipid droplets

Lipid droplets (LDs) are the primary cellular storage reservoir for fatty acids and cholesterol. LDs are large and stable in adipocytes, but smaller and transient LDs are present in most cell types (Fujimoto and Parton, 2011). LDs have a single phospholipid layer surrounding a neutral lipid core, primarily composed of triglycerides (TGs) and cholesterol esters (Olzmann and Carvalho, 2019). LDs form when individual fatty acids are enzymatically fused to a glycerol backbone to form neutral lipids (e.g. TG), which are inserted between membrane leaflets at specialized regions of the ER. In animal cells, large LDs bud from the ER and can remain for extended periods of time (Walther et al., 2017). Recruitment of specific lipases to the LD surface reverses this process, freeing lipids and individual fatty acids for use by the cell. LD lipases include adipose triglyceride lipase (ATGL), which generally cleaves the initial fatty acyl chain from TG leaving diacylglycerol (DG) (Zimmermann et al., 2004), and Hormone-sensitive lipase (Hsl), which cleaves a fatty acid from DG leaving monoacylglycerol (MG), and MG lipase, which cleaves the remaining fatty acid, freeing the glycerol backbone (Lass et al., 2011). Thus, LD-stored TG can supply individual fatty acids, but LDs are also a source for TG, DG and MG needed for cellular functions. The primary regulators of lipases at the LD surface are the Perilipin (PLIN) proteins (Jackson, 2019). PLINs can suppress or enhance recruitment of lipases (Ducharme and Bickel, 2008; Itabe et al., 2017).

Peroxisomes and LDs interact to facilitate cellular lipid metabolism

Organelles can coordinate their activities to facilitate overall cellular homeostasis. This includes peroxisomes and LDs, which both play crucial roles in regulating cellular lipids (Lodhi and Semenkovich, 2014; Thiam and Dugail, 2019). The metabolic functions of peroxisomes and LDs overlap via common metabolites or their intermediates (Choudhary and Schneiter, 2021; Lodhi and

[1]Department of Cell Biology, Faculty of Medicine and Dentistry, University of Alberta, Edmonton, AB T6G 2H7, Canada. [2]Future Fields, 11130 105 Ave NW, Edmonton, AB T5H 0L5, Canada. [3]Department of Medical Genetics, Faculty of Medicine and Dentistry, University of Alberta, Edmonton, AB T6G 2H7, Canada. *These authors contributed equally to this work

‡Author for correspondence (andrew.simmonds@ualberta.ca)

A.J.S., 0000-0001-7165-9302

Handling Editor: James Olzmann
Received 2 July 2021; Accepted 20 February 2022

Journal of Cell Science (2022) 135, jcs259092. doi:10.1242/jcs.259092

Semenkovich, 2014; Thiam and Dugail, 2019). Both organelles also require membrane contribution from the ER via specialized domains (Joshi and Cohen, 2019). In yeast cells grown in excess lipid, peroxisomes associate with newly forming LDs that remain at the ER (Binns et al., 2006). In COS7 cells, clusters of mature peroxisomes were observed near the LD surface (Schrader, 2001). LD-resident spastin M1 protein interacts with peroxisome ATP-binding cassette subfamily D member 1 (ABCD1) to promote interaction of peroxisomes with LDs (Chang et al., 2019). In *Caenorhabditis elegans*, PEX-5 mediates ATGL translocation to LDs, facilitating fasting-induced TG lipolysis (Kong et al., 2020). Finally, PEX2 was identified as part of a regulatory loop that couples ATGL activity to peroxisomal β-oxidation and reactive oxygen production (Ding et al., 2021).

Drosophila peroxisomes and LDs are conserved

The *Drosophila* homologs of the human PEX and yeast Pexp proteins are highly conserved (Anderson-Baron and Simmonds, 2019; Pridie et al., 2020; Mast et al., 2011), except that *Drosophila* peroxisome import does not employ an alternative pathway mediated by the PTS2 motif, recognized by Pex7. Notably, Pex7 requires docking with Pex5 to complete the process of protein import into the peroxisome (Kunze, 2020). Functionally, *Drosophila* peroxisomes are required for both VLCFA metabolism as well as managing reactive oxygen species (ROS) (Di Cara et al., 2017; Faust et al., 2014; Nakayama et al., 2011). Similarly, enzymes and regulatory proteins involved in LD formation and lipolysis are also highly conserved in flies (Heier and Kühnlein, 2018), as is the process of LD formation (Kuhnlein, 2012). Although protein families are conserved, the total number of LD regulatory proteins in *Drosophila* is less than that in mammals. Flies have only two PLINs: *Lsd-1* and *Lsd-2* (Beller et al., 2006; Bi et al., 2012; Guo et al., 2008). Upon phosphorylation, Lsd-1 facilitates lipid mobilization by recruiting *Drosophila* Hsl to the LD surface, facilitating lipolysis (Bi et al., 2012). Lsd-2 serves to protect the surface of LDs from lipases, such as the *Drosophila* ATGL homolog Brummer (Bmm) (Grönke et al., 2005). Embryonically derived *Drosophila* Schneider 2 (S2) cells have been used extensively to study LDs as they rapidly form multiple LDs when cultured in oleic acid (Beller et al., 2010; Guo et al., 2008; Kory et al., 2015; Krahmer et al., 2011; Sui et al., 2018; Wang et al., 2016; Wilfling et al., 2014, 2013). However, despite clear requirements for LDs during *Drosophila* development (Heier and Kühnlein, 2018), and conservation of Pex proteins and peroxisome metabolism (Anderson-Baron and Simmonds, 2019), little is known about how these organelles coordinate their activities.

Drosophila Pex gene mutations lead to altered levels of circulating fatty acids in larvae, causing developmental defects. These may be related to stored lipid availability, as altering the fatty acid in the larval diet can suppress some phenotypes associated with Pex gene mutations (Bülow et al., 2018; Chen et al., 2010; Di Cara et al., 2019; Liu et al., 2021; Sellin et al., 2018). The wide variety of lipids needed for cell structure, metabolism and energy storage during *Drosophila* development can be synthesized *de novo* or obtained by feeding (Heier and Kühnlein, 2018). The fat body constitutes a significant proportion of the larval body and is the major storage location for lipids (Church and Robertson, 1966; Musselman and Kuhnlein, 2018). *Drosophila* larvae feed almost constantly, storing TGs in the fat body (Heier and Kühnlein, 2018). Subsequent pupal development depends on fat body TG stores until the adult emerges from the pupa and begins to feed again (Musselman and Kuhnlein, 2018). The proportion of the larval fat body within a larva can be rapidly assayed by a simple buoyancy assay (Reis et al., 2010). To probe the requirements for peroxisomes during this stage of *Drosophila* development, we performed targeted RNA interference (RNAi) knockdown of Pex genes (*Pex*i) in the larval fat body. Although *Pex*i had the expected effect of inhibiting peroxisome proliferation, we noted that a few Pex genes had much stronger effects on lipid storage than others. To understand the underlying mechanism for how these few Pex proteins affected lipid storage, we compared mRNA expression in *Drosophila* S2 cells that were serum starved, cultured with oleic acid (+Oleate) or serum starved in the presence of a chemical inhibitor of Catalase, the primary ROS metabolism enzyme in peroxisomes. Of the 11 Peroxins needed for peroxisome assembly, only *Pex2*, *Pex13* and *Pex14* showed significant changes in mRNA levels when these various conditions were compared pairwise. To probe the mechanisms underlying this more direct linkage of a subset of Pex proteins to lipid storage, we examined LD formation in S2 cells cultured with excess oleic acid. There was a novel activity associated with only three Pex proteins – Pex3, Pex13 and Pex14 – in that they surrounded LDs independently of markers that would indicate they were incorporated into peroxisomes. This association was enhanced by mutations or *Pex*i suppressing Pex16 or Pex19, the key proteins that mediate insertion of Pex13 and Pex14 into the peroxisome bilayer membrane. Given that *Pex14* was altered in differential RNA sequencing (RNASeq) comparison of serum-starved cells to those fed excess oleic acid. *Pex14* knockdown had the strongest effect in the fat body; we focused on Pex14 in terms of LD function. We found that recruitment of Pex14 to LDs promotes TG storage and suppresses lipolysis, especially as cells transition from storing to releasing LD-stored fatty acids via lipolysis.

RESULTS

RNAi of Pex genes in the *Drosophila* fat body differentially affects lipid storage

To characterize requirements for peroxisome activity in the fat body, we performed a systematic *Pex*i screen, targeting each Pex gene via fat body-targeted transgenes (Fig. 1A,B; Fig. S1). Fat body-targeted *Pex14*i, and *Pex16*i, had much larger effects on larval buoyancy; *Pex19*i had almost no effect (Fig. 1C). Fat body *Pex14*i had the strongest effect on buoyancy and was coupled with a significant reduction in TG, as measured by a glycerol assay, compared to control (P<0.01) (Fig. 1D). Most (>80%) larvae with targeted *Pex*i in the fat body survived to pupal stage on standard cornmeal media (Fig. 1E), suggesting that extensive peroxisome biogenesis is not prevalent in larval fat body cells. To examine the role of dietary lipids on the fat body-targeted *Pex*i phenotypes, second-instar, feeding-stage larvae were transferred to a lipid-reduced diet (Piper et al., 2014). Fat body *Pex*i larvae raised on a lipid-reduced (holidic) medium survived less well than control larvae, with the strongest effects seen with *Pex3*i (50% survival), *Pex14*i (80% survival) or *Pex19*i (60–90% survival) (Fig. 1E). Larvae will consume a lipid-enriched diet containing lard (Woodcock et al., 2015). When larvae were fed holidic food plus lard, the survival rate of *Pex3*i larvae was also lower than that of control larvae (30%; Fig. 1E). Fat body-targeted *Pex13*i (15–20%, P<0.01) or *Pex14*i (15–20%, P<0.001) significantly reduced larval survival on lard food (Fig. 1E). Neutral lipid staining showed LDs filling each cell, with peroxisomes distributed throughout the cytoplasm (Fig. 1F, LipidTOX). The Pex14 protein had two patterns of cellular localization; the first was punctate sites enriched in proteins with the SKL (PTS1) motif (Fig. 1F, SKL). Pex14 was also observed surrounding the LDs in a pattern that did not overlap with SKL (Fig. 1F, Pex14). In *Pex14*i larvae, Pex14 signal and mature peroxisomes (punctate SKL) were

Journal of Cell Science (2022) 135, jcs259092. doi:10.1242/jcs.259092

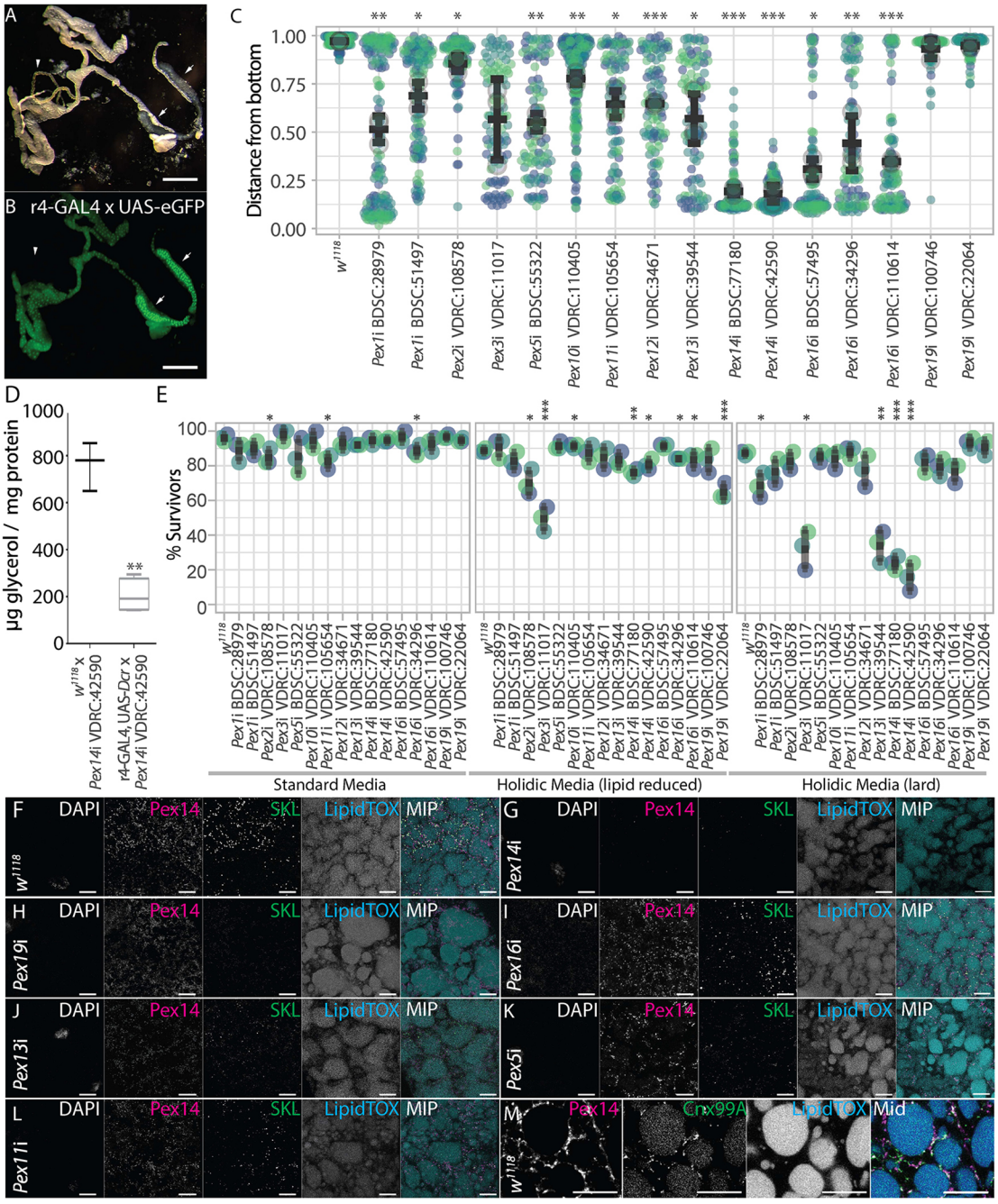

Fig. 1. Targeted knockdown of Pex genes in the larval fat body has differential effects on LD formation. (A) *Drosophila* larval third-instar fat body and salivary glands (arrows), and Malpighian tubules (arrowhead). (B) r4-GAL4:UAS-*Dcr*, UAS-GFP is expressed strongly in fat body and salivary glands (arrows) but not in Malpighian tubules (arrowhead). (C) Greater r4-GAL4:UAS-*Dcr* >*Pex*i effects on fat body formation caused larvae to sink in a sucrose solution (mean±95% c.i.; **P*<0.05, ***P*<0.01 and ****P*<0.001; unpaired Welch's *t*-test). (D) r4-GAL4:UAS-*Dcr*>*Pex14*i VDRC:42590 (*Pex14*i) significantly reduced triacylglycerol levels. The box represents the 25-75th percentiles, and the median is indicated (box too small to show on left). The whiskers show the 5-95th percentiles (***P*<0.01; unpaired Welch's *t*-test). (E) Lethality caused by fat body *Pex13*i and *Pex14*i was enhanced by excess dietary fat (mean±s.d.; **P*<0.05, ***P*<0.01 and ****P*<0.001; Shaprio-Wilk test). (F) Maximum intensity projection (MIP) images of r4-GAL4:UAS-*Dcr* x *w*^{1118} fat body cells show uniformly sized and tightly packed lipid droplets (LDs) (LipidTox), and multiple peroxisomes (punctate SKL). Most Pex14 overlapped peroxisomes (punctate SKL) but some surrounded LDs independently of SKL. (G) r4-GAL4:UAS-*Dcr*>*Pex14*i VDRC:42590 (*Pex14*i) cells had very few peroxisomes and fewer, more variably sized LDs. (H) r4-GAL4:UAS-*Dcr*>*Pex19* VDRC:22064 (*Pex19*i) fat body cells had large LDs surrounded by Pex14 and few peroxisomes. (I) Fat body cells from r4-GAL4:UAS-*Dcr*>*Pex16* VDRC:110614 KK (*Pex16*i); larvae had smaller LDs, but Pex14 was recruited to peroxisomes and surrounded LDs. (J) LDs in r4-GAL4:UAS-*Dcr*>*Pex13* VDRC:39544 (*Pex13*i) fat body cells were like wild type, but fewer peroxisomes were present. Relatively less Pex14 surrounded LDs. (K) r4-GAL4:UAS-*Dcr*>*Pex5* BDSC:55322 (*Pex5*i) fat body cells had smaller LDs that were surrounded by Pex14 and fewer peroxisomes. (L) LDs were smaller and more numerous in r4-GAL4:UAS-*Dcr*>*Pex11* VDRC:105654 (*Pex11*i) fat body cells, while Pex14 localization to peroxisomes was like wild type. (M) Some of the Pex14 surrounding LDs overlapped with endoplasmic reticulum (ER) (Cnx99A). Scale bars: 5 µm.

largely absent (Fig. 1G). The LDs in the *Pex14*i fat body appeared smaller and were fewer in number than those in control fat body (Fig. 1G). *Pex19*i fat body LDs were larger, and peroxisomes were absent (Fig. 1H). In *Pex19*i fat body cells, Pex14 surrounded very-large LDs (Fig. 1H). Enlargement of LDs and reduced peroxisome number were seen in *Pex16*i fat body (Fig. 1I),

Journal of Cell Science

Journal of Cell Science (2022) 135, jcs259092. doi:10.1242/jcs.259092

although to a lesser extent than in *Pex19*i fat body. *Pex13*i and *Pex5*i fat body had reduced peroxisome abundance and increased Pex14 signal adjacent to LDs (Fig. 1J,K). *Pex11*i fat body cells had a pattern of LDs and peroxisomes like that of control fat body cells (Fig. 1L). The fewer number of peroxisomes (punctate SKL) would be expected in *Pex11*i cells as the primary role of Pex11 is regulating fission of existing peroxisomes (Schrader et al., 2016). Some of the Pex14 signal surrounding LDs in fat body cells colocalized with Calnexin 99A (Cnx99A), an ER marker, but considerable ER-independent Pex14 signal surrounding LDs was also present (Fig. 1M).

RNASeq of S2 cells cultured in conditions promoting LD formation or starvation

Drosophila S2 cells form LDs consistent in both number and volume (Guo et al., 2008) when the culture medium is supplemented with oleic acid, an 18-carbon monounsaturated fatty acid (Darfler, 1990). Omitting serum from standard Schneider's medium (serum starved) induced a starvation response and increased the level of mRNAs encoding proteins involved in ROS and reactive nitrogen species (RNS) production (Fig. 2A; Table S1). *Lsd-1* was significantly different [$P<0.05$, adjusted P (Padj)<0.1], and *Pex2* and *bmm* were also different but at lower confidence (Padj>0.1). However, comparison of serum-starved to +Oleate cultured cells showed the greatest change in mRNAs of pathways affecting fatty acid metabolism and peroxisomal protein import, including *Pex14* (Fig. 2B; Table S2). Other comparisons of serum-starved, standard and oleic acid culture showed changes in multiple genes previously associated with LDs (Figs S2 and S3). Notably, of all Pex genes, only *Pex14* levels were significantly differently (Padj<0.1) enriched in S2 cells cultured in +Oleate condition compared to serum starvation condition. To address the potential effect of peroxisome ROS metabolism in the observed effects, RNASeq was also performed on serum-starved cells treated with 3-amino-1,2,4-triazole (3AT), which suppresses Catalase (Samis et al., 1972). Notably, very few mRNAs had different levels in serum-starved versus serum-starved +3AT cells (Table S4), suggesting that ROS metabolism is not linked to response to starvation or oleic acid in S2 cells (Table S1). Comparing serum-starved +3AT cells with those in standard culture showed (Table S5) differences in *Lsd-1* and *Pex13* at high confidence and *Pex11ab* at lower confidence (Padj>0.1), while comparison with +Oleate cells (Table S6) showed *Pex14* changes at high confidence and *Lsd-1* at lower confidence (Padj>0.1). For all comparisons, high-confidence changes in mRNAs encoding genes known to encode LD-resident or regulatory proteins (Beller et al., 2006; Cermelli et al., 2006; Guo et al., 2008) were present (Tables S1–S6).

The observed changes in mRNA levels of a subset of peroxisome protein import genes did not correlate with a corresponding increase in other Pex genes required for peroxisome proliferation. To confirm whether these Pex genes were linked to conditions that would alter the formation/lipolysis of LDs, we compared expression of each when +Oleate cells were subsequently transferred to serum-starved culture for 24 h, which would induce lipolysis of LD-stored TGs (lipolytic). The increased level of *Pex14* in +Oleate cells was not maintained when cells were induced to metabolize LD-stored neutral lipids by transfer to serum-starved conditions (Lipolytic, Fig. 2C). The relative increase in *Pex14* mRNA levels in +Oleate cultured cells was coupled with an increase in Pex14 protein (Fig. 2D). The relative change in Pex14 protein level was less than that seen at the mRNA level by quantitative reverse transcription PCR (qRTPCR), but this may be due to post-transcriptional regulation of the *Pex14* mRNA (Dahan et al., 2022).

Pex14 localizes to LDs when S2 cells are cultured in +Oleate conditions

When S2 cells were cultured in standard conditions, mature peroxisomes (punctate SKL) and Pex14 largely overlapped (Fig. 2E). In +Oleate cultured S2 cells, Pex14 could be observed surrounding LDs. This signal did not overlap peroxisomes (punctate SKL, Fig. 2F). When S2 cells were subsequently placed in lipolytic conditions, Pex14 surrounded larger LDs (Fig. 2G). Quantification of three-dimensional colocalization showed that peroxisome numbers were relatively similar in cells cultured under standard, +Oleate and lipolytic conditions (Fig. 2H). In both fat body and S2 cells, the Pex14 surrounding LDs was independent of Abcd3, a non-Peroxin PMP inserted into the peroxisome membrane (Fig. S4A–D), and the punctate SKL that marks proteins concentrated inside mature peroxisomes (Fig. S4E–I). Pex14 protein was present in isolated LD fractions from *Pex19* knockout (KO) S2R+ cells lacking peroxisomes (Fig. 2I). Notably, LD-associated Pex14 was resistant to alkaline carbonate treatment (Fig. 2I,J), indicating that Pex14 has a stable association with the LD surface.

*Pex14*i alters TG lipolysis and LD morphology

In *Pex14*i S2 cells, PTS1-mediated (SKL) peroxisomal import was reduced (Baron et al., 2016). *Pex14*i affected peroxisome volume and number in +Oleate and lipolytic cultured S2 cells as well as influenced LD volume and number (Fig. 3A–H). Peroxisome volume was significantly reduced ($P<0.01$) in +Oleate *Pex14*i cells but had little effect in cells in lipolytic conditions (Fig. 3E). Conversely, *Pex14*i had little effect on peroxisome number in +Oleate cultured cells but a significant effect on peroxisome number in cells in lipolytic conditions ($P<0.01$, Fig. 3F). Changes in LD number and volume have been shown previously to correlate strongly with changes in TG storage in S2 cells (Guo et al., 2008). *Pex14*i had relatively small effects on LD volume or number in +Oleate cultured cells but caused LD fragmentation (increased number and smaller volume) when cells were transferred to lipolytic conditions (Fig. 3G,H). TG lipolysis is also reflected in changes in free glycerol levels in cell lysates (Tennessen et al., 2014). *Pex14*i led to an increase in lipolysis in lipolytic culture conditions (Fig. 3I), coupled with reduced peroxisome proliferation (Fig. 3F). *Pex14*i efficacy of >90% was confirmed by qRTPCR (Fig. 3J).

Peroxisome formation in *Drosophila* requires the collective activity of 11 conserved Pex proteins (Anderson-Baron and Simmonds, 2019; Baron et al., 2016; Faust et al., 2012). Peroxisomes have a half-life of ∼2 days (Nordgren et al., 2013), and it is unlikely Pex14 is released once incorporated into the peroxisomal membrane (Natsuyama et al., 2013). Myc-tagged Pex14 surrounds peroxisomes in standard culture (Fig. 3K) and surrounds newly formed LDs after +Oleate culture (Fig. 3L). To determine whether the Pex14 surrounding newly formed LDs was newly translated from the increased *Pex14* mRNA, we performed pulse-chase protein labeling. Myc-Pex14 transfected cells were incubated with ^{35}S-Met immediately after transfection (0–24 h) or 24 h after transfection (24–72 h). Cells that were labeled immediately after transfection were washed after 24 h to remove excess ^{35}S-Met. Autoradiography of total labeled protein from the LD fraction of control and +Oleate cultured cells pulse labeled at 0 h showed that only a few newly synthesized proteins were recruited to LDs in cells grown in +Oleate culture. This increased over time in

Journal of Cell Science (2022) 135, jcs259092. doi:10.1242/jcs.259092

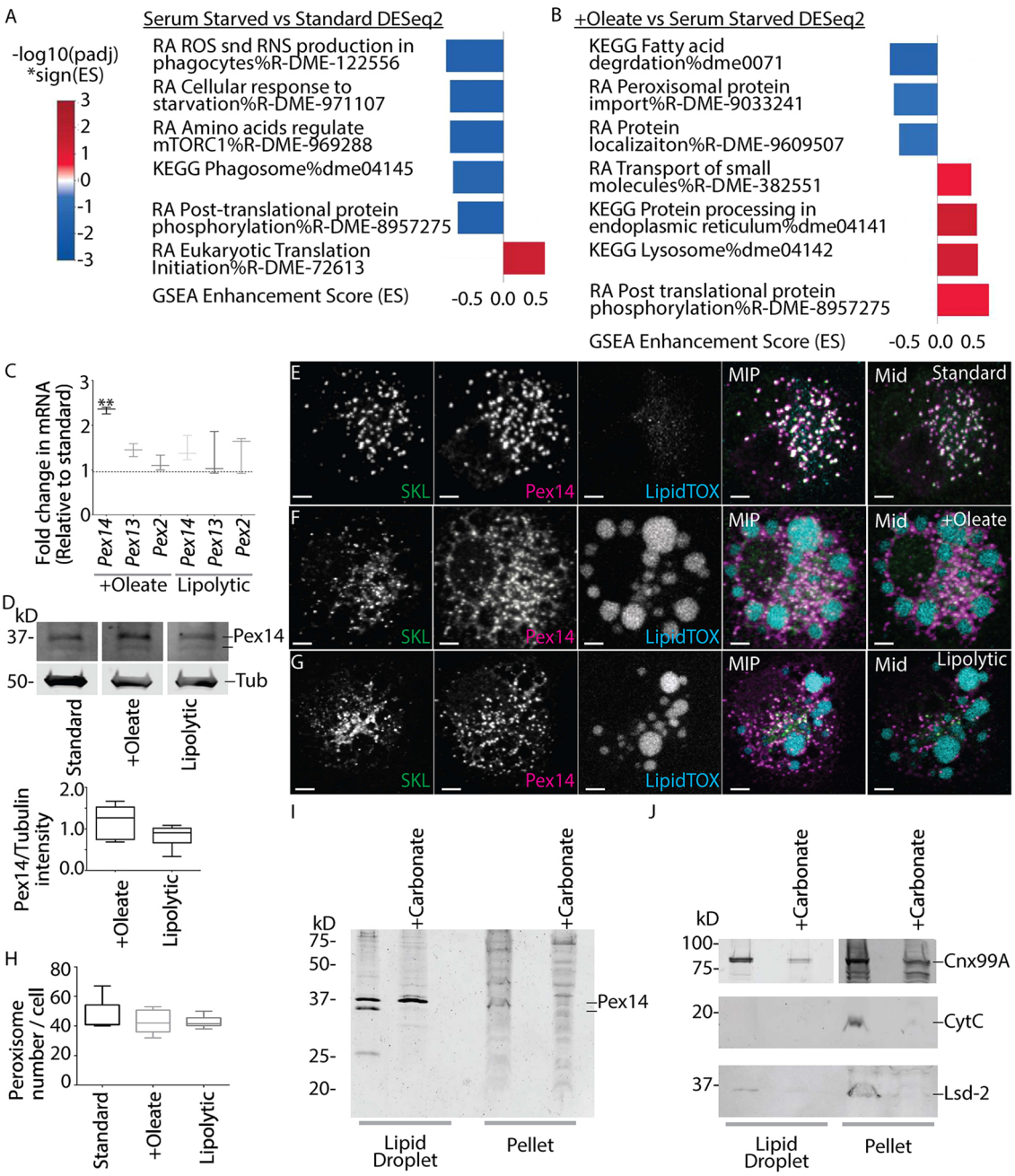

Fig. 2. Differential whole-genome RNASeq identified Pex14 as uniquely upregulated and LD associated in S2 cells cultured in +Oleate conditions. (A) Gene set enrichment analysis (GSEA) of the results of differential RNA sequencing (RNASeq) of S2 cells cultured in Schneider's medium supplemented with FBS (Standard) compared to culture in unsupplemented medium (Serum Starved) indicated changes in mRNAs encoding proteins needed for reactive oxygen species (ROS)/reactive nitrogen species (RNS) production in phagocytes, and mTORC and other pathways that would be expected to change in response to starvation. (B) Comparing serum-starved cells to those cultured in +Oleate medium showed changes in mRNA needed for fatty acid metabolism and peroxisome protein import. (C) Quantitative reverse transcription PCR (qRTPCR) analysis of the three Pex mRNAs that had significant changes in RNASeq under any conditions revealed that only *Pex14* was strongly elevated in +Oleate conditions (mean±s.d. $^{**}P<0.01$; unpaired two-tailed Student's *t*-test). (D) Elevated *Pex14* mRNA in +Oleate cells correlated with increased protein levels. (E) In standard cultured S2 cells, some Pex14 signal largely overlapped peroxisomes (punctate SKL). (F) In +Oleate culture, the Pex14 signal also surrounded LDs (LipidTox). (G) When LD lipolysis was induced by transfer of +Oleate cultured cells to serum-starved conditions (Lipolytic), LD fragmentation occurred. (H) The relative number of peroxisomes was the same in cells cultured in standard, +Oleate or lipolytic conditions. (I) Pex14 was present in the LD fraction of *Pex19*KO S2R+ cells (+Oleate) even after alkaline carbonate treatment (+Carbonate). (J) Markers for ER (Cnx99A) or mitochondria (CytC) were largely absent from +Carbonate LD fractions. For, D and H, the box represents the 25-75th percentiles, and the median is indicated. The whiskers show the 5-95th percentiles. Scale bars: 2 µm.

+Oleate culture with a prominent band at 45 kD (Fig. 3M). In addition, 6xMyc-Pex14 immunoprecipitation/autoradiography showed that newly translated Pex14 was recruited to LDs (Fig. 3N). Pex14 surrounded large LDs when cells were transferred from +Oleate to lipolytic conditions (Fig. 3O).

Pex14 is more strongly recruited to LDs in *Pex19*KO cells

Pex19 mediates Pex13 and Pex14 insertion into bilayer membranes that contain Pex3 (Itoh and Fujiki, 2006). Pex14 can associate with mitochondrial membranes when Pex19 is absent (Sacksteder et al., 2000). In +Oleate cultured, *Pex19*KO, S2R+ cells, the majority of

Journal of Cell Science (2022) 135, jcs259092. doi:10.1242/jcs.259092

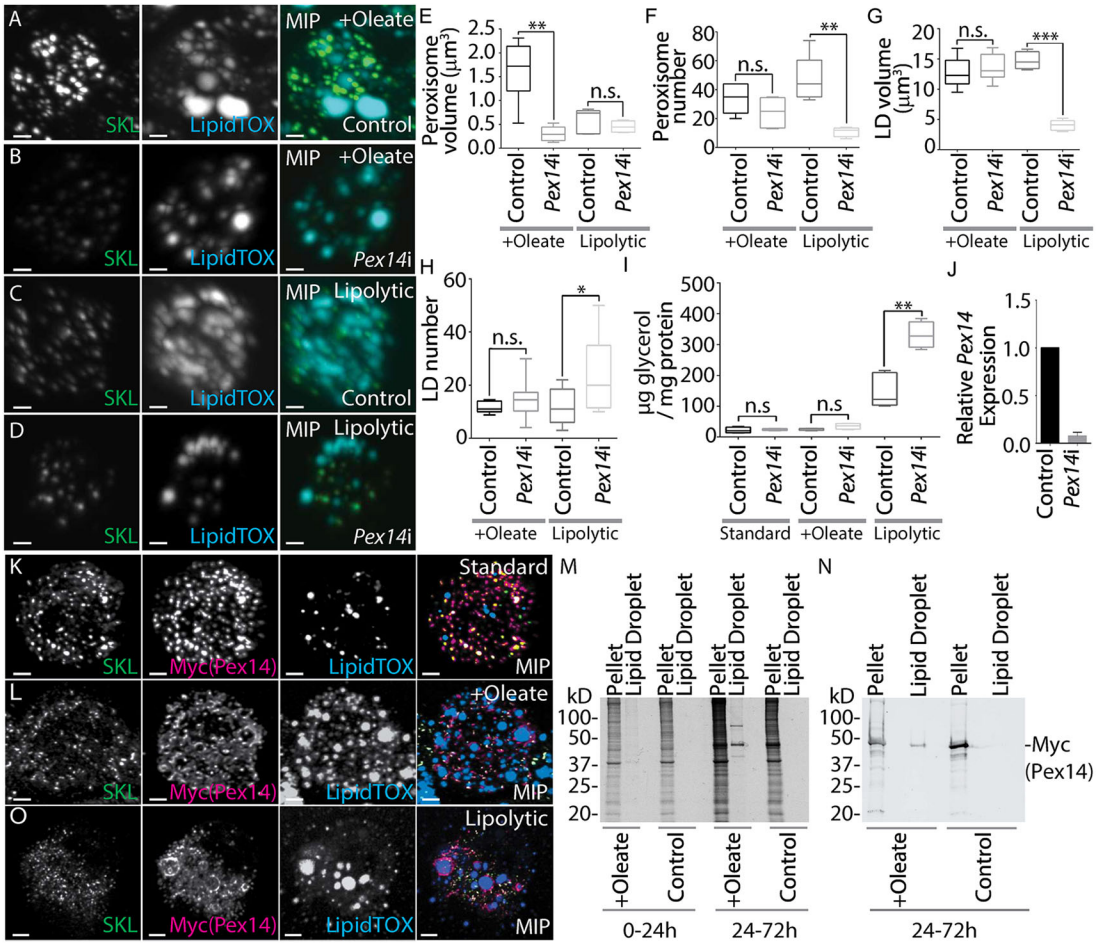

Fig. 3. *Pex14*i affects peroxisomes as well as LD formation and lipolysis. (A) +Oleate cultured S2 cells treated with scrambled dsRNA (Control). (B) *Pex14* RNAi (*Pex14*i) of +Oleate S2 cells. (C) S2 cells cultured in lipolytic conditions treated with scrambled dsRNA (Control). (D) *Pex14*i cells in lipolytic conditions. (E) The average volume of peroxisomes per *Pex14*i cell cultured under +Oleate conditions was significantly less than that of control cells and lipolytic cultured cells (**P<0.01; unpaired two-tailed Student's t-test). (F) +Oleate *Pex14*i cells had ∼30–40 peroxisomes, as did untreated cells, but *Pex14*i cells cultured in lipolytic conditions had an average of five to ten peroxisomes (**P<0.01; unpaired two-tailed Student's t-test). (G) The average volume of LDs was similar in +Oleate control and *Pex14*i cells. In lipolytic conditions, LDs were significantly smaller in *Pex14*i cells relative to control cells (***P<0.001; unpaired two-tailed Student's t-test). (H) The average number of LDs per lipolytic cultured *Pex14*i cell was higher than that in control cells (*P<0.05; unpaired two-tailed Student's t-test). (I) Triglyceride (TG) lipolysis increased in lipolytic culture conditions in *Pex14*i cells (**P<0.01; unpaired two-tailed Student's t-test). (J) qRTPCR confirmed >90% knockdown *Pex14*i efficiency. Results are mean±s.d. (K) Myc-tagged Pex14 overexpressed in standard cultured S2 cells colocalized with peroxisomes (punctate SKL) with only few LDs (LipidTOX) present. (L) +Oleate cultured cells induced formation of large LDs surrounded by Myc-Pex14. (M) Autoradiography of total protein extracts from pellet or LD fractions following a ^{35}S-Met 24 h pulse-chase labeling as cells were transferred to +Oleate culture. (N) Western blot of Myc immunoprecipitation from 24–72 h LD fractions showed that the proportion of Myc-Pex14 in the LD fraction is relatively higher in +Oleate cultured cells. (O) In S2 cells cultured in lipolytic conditions, Myc-Pex14 was observed surrounding large LDs. For box plots in E-I, the box represents the 25-75th percentiles, and the median is indicated. The whiskers show the 5-95th percentiles. Scale bars: 2 µm. n.s., not significant.

Pex14 LDs was associated with LDs (Fig. 4A), similar to *Pex19*i fat body (Fig. 1H). Confocal imaging showed that Pex14 was near ER surrounding LDs (Fig. 4A; Fig. S5A). However, Pex14 surrounding LDs did not appreciably colocalize with Cytochrome-C (CytC), which marks mitochondria (Fig. 4B; Fig. S5B). *Pex19*KO S2R+ cells co-expressed mNeonGreen-SKL, which was dispersed throughout the cell, indicating that the Pex13/Pex14-mediated peroxisome matrix protein import was absent. Using super-resolution (30 nm) stimulated emission depletion (STED) imaging, we found that Pex14 surrounding LDs was largely overlapping with a protein marker for the LD surface (Fig. 4C, LiveDrop) (Wang et al., 2016). The relative spatial relationship of Pex14 and Cnx99A (ER) at the LD surface (LiveDrop-GFP) at 30 nm resolution was examined in S2 cells stably expressing LiveDrop-GFP, which suggested that Pex14 was more closely associated with the surface of LDs than the surrounding ER (Fig. 4D).

Pex14 at the LD affects recruitment of Hsl

mRNAs encoding LD-associated proteins like Hsl and Lsd-2 were significantly altered (P<0.05, Padj/FDR<0.1) in S2 cells cultured in +Oleate compared to serum-starved conditions, as were those encoding Pex3 and Pex13 (Tables S2 and S6). Overexpression of Bmm in S2 cells caused rapid LD fragmentation, indicating increased lipolysis (Fig. 5A). When Pex14 was co-overexpressed in these cells, LD fragmentation also occurred (Fig. 5B). Overexpression of Hsl similarly caused LD fragmentation, but this was suppressed when Pex14 was overexpressed in the same cells (Fig. 5C,D). Co-overexpression of Pex13 and Hsl also suppressed LD fragmentation to a lesser extent (Fig. S5C,D). Three-dimensional quantification of relative protein localization in these cells showed that Pex14 was concentrated in a region immediately adjacent to LDs, where more than 50% of the signal corresponding to overexpressed Bmm and Hsl lipase was concentrated (Fig. 5B,D,E). However, in lipolytic

Journal of Cell Science (2022) 135, jcs259092. doi:10.1242/jcs.259092

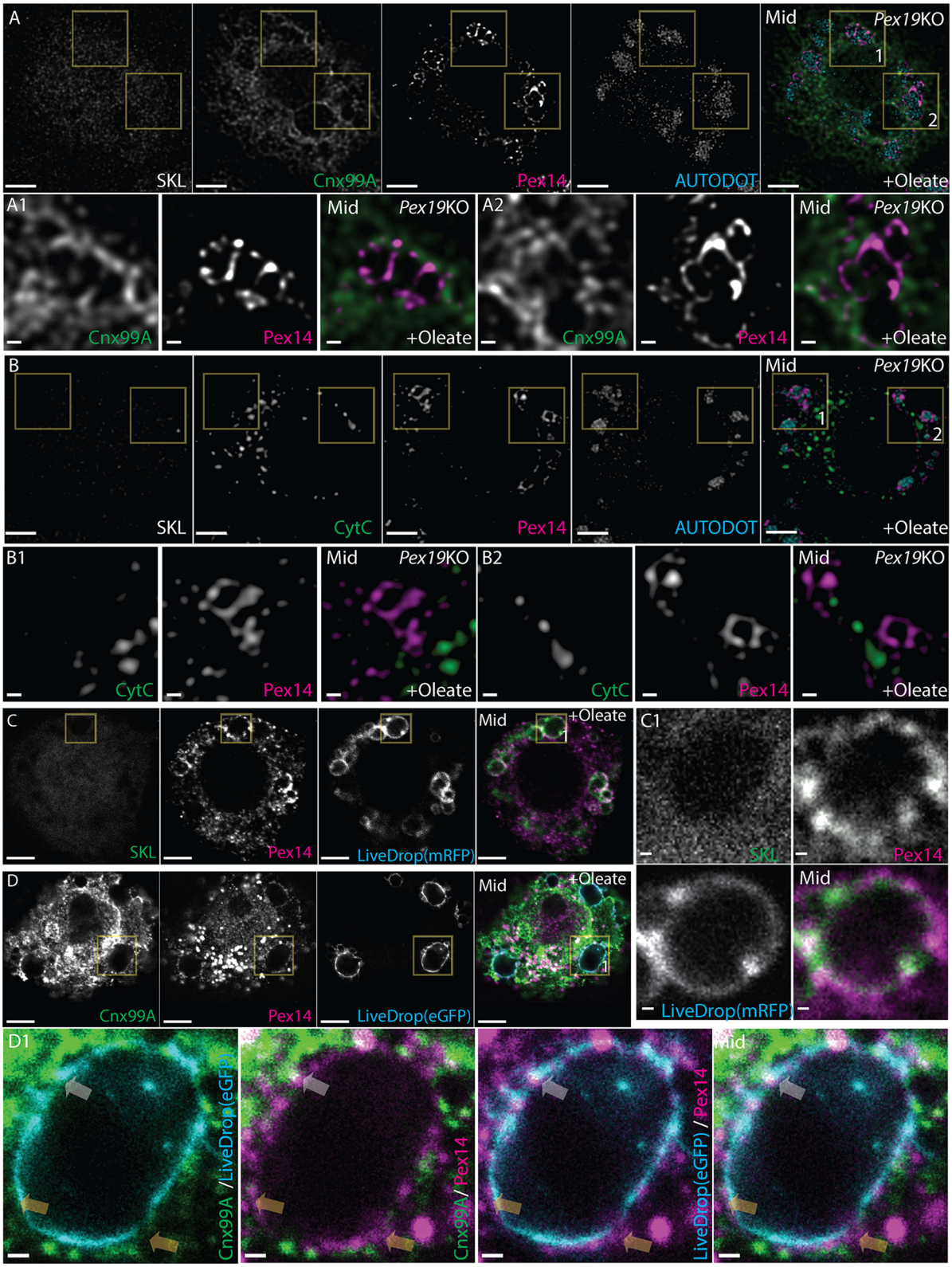

Fig. 4. Comparison of endogenous Pex14 localization relative to LDs, ER and mitochondria. (A) Single confocal plane images (Mid) of *Pex19*KO S2R+ cell constitutively expressing mNeonGreen-SKL. No mature peroxisomes (SKL punctate) were observed. Endogenous Pex14 surrounded LDs (AUTODOT). Zoomed regions (A1,A2) showed that some Pex14 surrounding LDs overlapped with ER (Cnx99A) but most did not. (B) There was no colocalization between Pex14 and a mitochondrial marker (CytC) even in high-magnification zoom (B1,B2) images of single planes in the middle of the cell. (C) Two-color stimulated emission depletion (STED) images (30 nm lateral resolution) show overlapping colocalization of Pex14 with the LiveDrop-RFP in *Pex19*KO cells. (C1) High-magnification zooms showed considerable overlap between the Pex14 and LiveDrop signals. (D) Three-color STED imaging of S2 cells stably expressing LiveDrop-GFP show large Pex14 punctate (peroxisomes) and some proportion of small Pex14 punctate surrounding LDs. (D1) Pex14 is between the ER–LD interface (white arrows) and colocalized with the LD surface independently of the ER (yellow arrows). Scale bars: 2 µm (A–D) and 0.5 µm (A1,A2,C1,D1,B1,B2).

Journal of Cell Science (2022) 135, jcs259092. doi:10.1242/jcs.259092

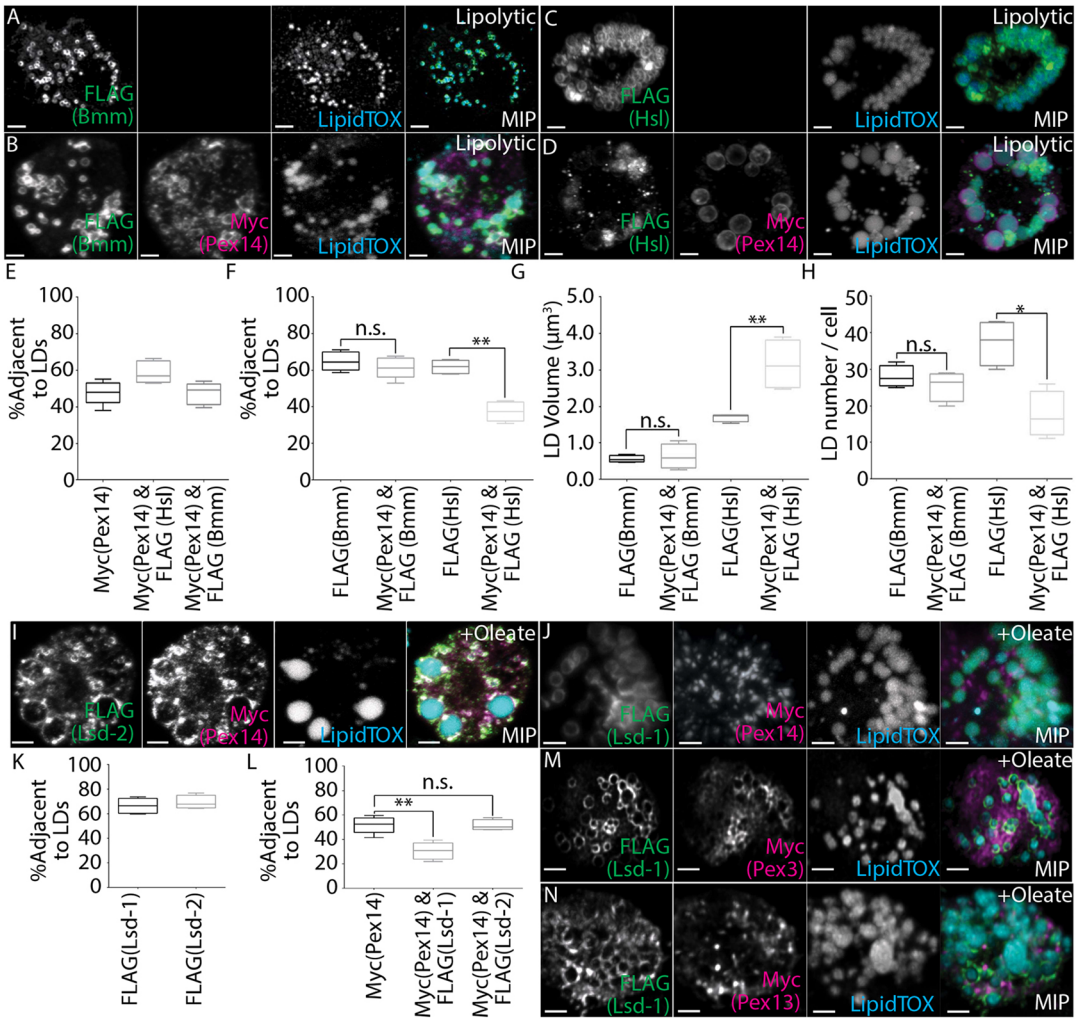

Fig. 5. Pex14 influences Hsl recruitment to LDs in cells cultured in lipolytic conditions. (A) 3xFLAG-Bmm (FLAG) in lipolytic cultured S2 cells surrounded multiple small LDs (LipidTOX). (B) LDs in lipolytic cultured S2 cells co-overexpressing 6xMyc-Pex14 and 3xFLAG-Bmm were similarly fragmented. (C) In lipolytic cultured S2 cells, 3xFLAG-Hsl also surrounded fragmenting LDs. (D) Co-overexpressing 6xMyc-Pex14 caused 3xFLAG-Hsl to be absent from the periphery of large LDs when Pex14 was present. (E) Myc-Pex14 recruitment to the region immediately surrounding LDs (% Adjacent) was largely unaffected by increased Bmm or Hsl. (F) Co-overexpressing Myc-Pex14 had little effect on Bmm association with LDs but the proportion of Hsl surrounding LDs was reduced by ∼30% (**P<0.01; unpaired two-tailed Student's t-test). (G) S2 cells co-overexpressing FLAG-Bmm and Myc-Pex14 showed no change in LD volume when transferred to lipolytic culture conditions. However, when co-overexpressing FLAG-Hsl and Myc-Pex14, average LD volumes were ∼1.7× larger (**P<0.01; unpaired two-tailed Student's t-test). (H) Co-overexpressing FLAG-Hsl and Myc-Pex14 suppressed LD fragmentation by ∼2-fold (*P<0.05; unpaired two-tailed Student's t-test), while little effect was observed with FLAG-Bmm overexpression. (I) Co-overexpressing 6xMyc-Pex14 and 3xFLAG-Lsd-2 led to increased LD volume in +Oleate cultured S2 cells. (J) In +Oleate cells co-overexpressing 6xMyc-Pex14 and 3xFLAG-Lsd-1, Myc-Pex14 was excluded from LDs. (K) 3xFLAG-Lsd-1 and 3xFLAG-Lsd-2 were both strongly recruited (>60%) to the region adjacent to LDs in +Oleate conditions. (L) Overexpression of Lsd-1 suppressed (–1.8×) recruitment of Pex14 to LDs (**P<0.01; unpaired two-tailed Student's t-test). (M,N) +Oleate S2 cells co-overexpressing 3xFLAG-Lsd-1 did not suppress 6xMyc-Pex3 (M) adjacent to LDs but suppressed 6xMyc-Pex13 (N). Images are MIPs of a whole cell volume. In all box plots, the box represents the 25-75th percentiles, and the median is indicated. The whiskers show the 5-95th percentiles. Scale bars: 2 µm. n.s., not significant.

conditions, although Pex14 and Bmm remained concentrated adjacent to LDs, there was a reduction in Hsl overlap when Pex14 was at high levels (Fig. 5D,F). Pex14-induced repression of Hsl surrounding LDs was linked to an increase in LD volume and decrease in number (Fig. 5C,D,G,H), suggesting suppression of Hsl-mediated lipolysis (Marcinkiewicz et al., 2006).

Although there is some overlap in *Drosophila* PLIN activities, it is thought that Lsd-1 facilitates LD lipid mobilization by Hsl while Lsd-2 suppresses Bmm-mediated lipolysis at LDs (Beller et al., 2010; Marcinkiewicz et al., 2006). Simultaneously overexpressing Pex14 and Lsd-2 resulted in both being largely adjacent to LDs (Fig. 5I). Conversely, co-overexpression of Pex14 and Lsd-1 resulted in suppression of Pex14 recruitment to LDs (Fig. 5J). Although overexpressed Lsd-1 or Lsd-2 are both strongly recruited to LDs (Fig. 5K), Lsd-1 significantly repressed Pex14 co-recruitment (P<0.01, Fig. 5L). Notably, whereas Pex3 localization to LDs was unaffected by Lsd-1 overexpression in +Oleate conditions, Pex13 was strongly affected (Fig. 5M,N).

A small region of Pex14 including the TM domain is sufficient for LD association

When inserted into the peroxisome bilayer membrane, PEX14 is proposed to have an N-in C-out topology (Barros-Barbosa et al., 2019; Reuter et al., 2021). Several N- or C-terminal truncations of Pex14 were tested for recruitment to LDs or peroxisomes in +Oleate cells (Fig. 6A). mRFP-tagged full-length Pex14$^{aa1–280}$ produces a punctate pattern indicating peroxisomes as well as strongly overlaps with LiveDrop-GFP in live-imaged S2 cells (Fig. 6B). The

Journal of Cell Science (2022) 135, jcs259092. doi:10.1242/jcs.259092

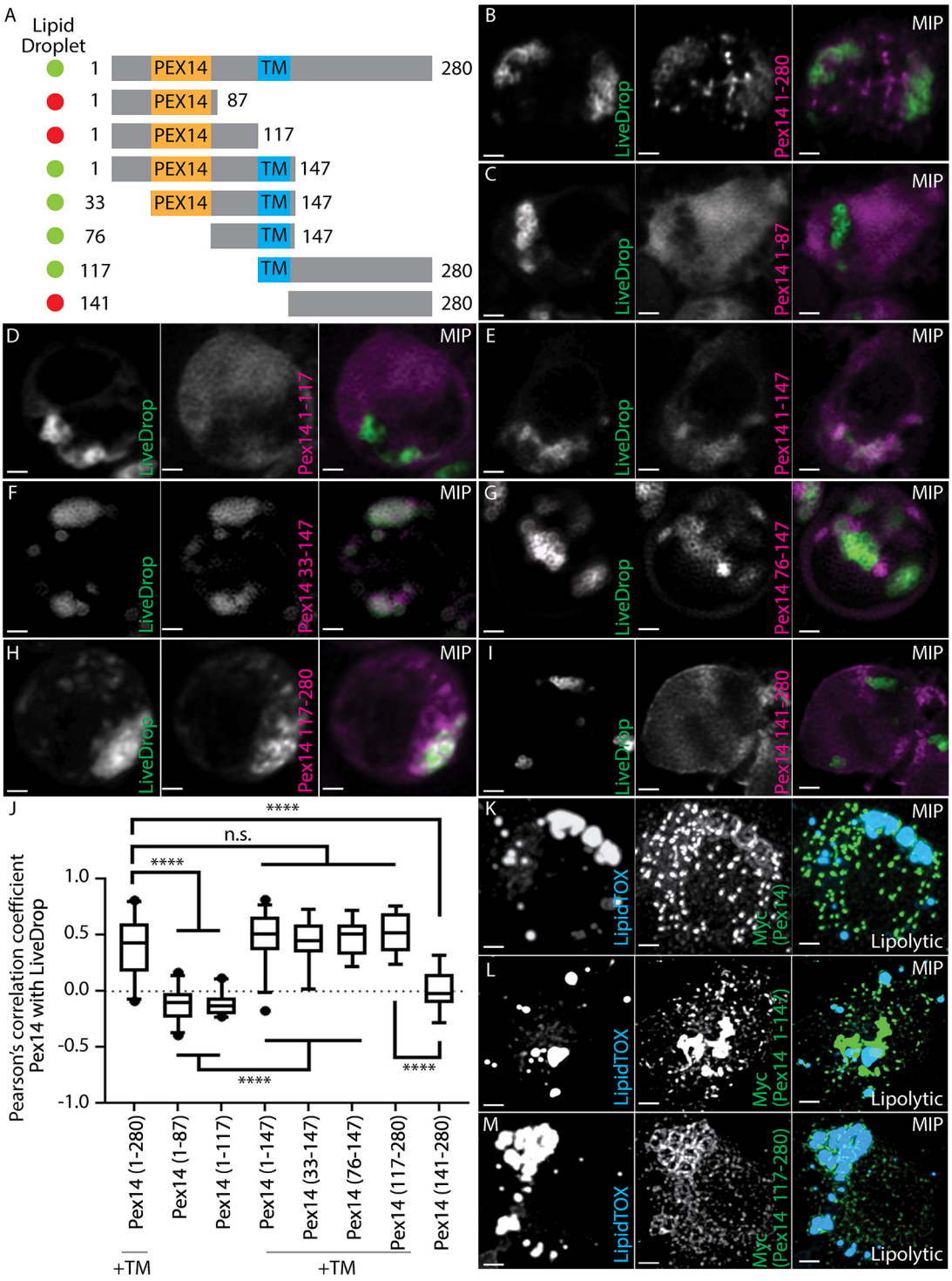

Fig. 6. The transmembrane domain is required for the recruitment of Pex14 to LDs. (A) *Drosophila Pex14* is 280 amino acids (aa) long and a conserved Pex14 domain (orange) and a single transmembrane (TM) domain (blue). Only those forms of Pex14 with the TM region are recruited to LDs (red/green circles). (B–I) Live imaging of +Oleate cultured S2 cells co-expressing the LD marker LiveDrop(GFP) and RFP-tagged Pex14 truncation mutations. The images shown are MIPs. (B) Full-length Pex14$^{aa1–280}$ overlapped with LiveDrop and formed punctate spots characteristic of peroxisomes. (C,D) Pex14$^{aa1–87}$ (C) and Pex14$^{aa1–117}$ (D) were homogeneously distributed throughout the cell. (E) Pex14$^{aa1–147}$ containing the TM domain colocalized with LiveDrop. (F,G) Pex14$^{aa33–147}$ (F) and Pex14$^{aa76–147}$ (G) colocalized with LiveDrop. (H) Pex14$^{aa117–280}$, which includes the TM domain, partially colocalized with LiveDrop. (I) Pex14$^{aa141–280}$ appeared to localize to the plasma membrane. (J) Pearson's correlation confirmed lack of Pex14$^{aa1–87}$, Pex14$^{aa1–117}$ and Pex14$^{aa141–280}$ colocalization with LiveDrop (****P<0.0001, Mann–Whitney test). Comparison of Pex14$^{aa1–87}$ or Pex14$^{aa1–117}$ to Pex14$^{aa1–147}$, Pex14$^{aa33–147}$ or Pex14$^{aa76–147}$ indicated significant differences (****P<0.0001, Kruskal–Wallis test). The box represents the 25-75th percentiles, and the median is indicated. The whiskers show the 5-95th percentiles. (K) In S2 cells co-expressing Hsl and Pex14, Pex14 localized to peroxisomes (punctate SKL) and surrounded LDs (LipidTOX). Despite elevated Hsl, LDs were not fragmented. (L) In cells co-expressing Hsl and an N-terminal Pex14$^{aa1-147}$, LDs were fragmented. (M) Pex14$^{aa117–280}$ surrounded large LDs and suppressed Hsl-mediated LD fragmentation. Scale bars: 2 µm. n.s., not significant.

Journal of Cell Science (2022) 135, jcs259092. doi:10.1242/jcs.259092

N-terminal 1–87 amino acids (aa) of Pex14 contain a region homologous to the 'PEX14' domain that mediates interaction with PEX5 and PEX13. This region was insufficient to mediate LD or peroxisome association and was relatively homogeneous within the cell (Fig. 6C). A longer truncated form of Pex14$^{aa1-117}$ including the N-terminal Pex14, but not the TM, domains was cytosolic (Fig. 6D). Inclusion of the predicted TM domain (aa119–141) of Pex14 retained LD association (Fig. 6E). Truncations beginning with the N-terminal end found that a region surrounding the TM domain (aa76–147) that did not include the Pex14 domain (aa34–75) or the C-terminal portion of the protein (aa117–280) was sufficient to mediate recruitment to LDs (Fig. 6F–H). The C-terminal of Pex14 missing the TM domain (aa141–280) does not surround LDs (Fig. 6I). In all cases, if the TM domain was not present, Pex14 truncations were not seen surrounding LDs (Fig. 6D,I). Only Pex14 transgenes that contained the TM domain were recruited to LDs (Fig. 6J). In S2 cells overexpressing Hsl, full-length Pex14 or truncations that contained both the TM domain and the C-terminal end suppressed Hsl-mediated LD fragmentation (Fig. 6K–M).

Reduction in Pex proteins that mediate Pex14 insertion in the peroxisome membrane enhances Pex14–LD association

To probe the linkage between the canonical role for Pex14 in peroxisome assembly and the newly identified role at LDs, we tested the effect of knockdown of Pex genes that affected different aspects of PMP insertion and enzyme import in S2 cells stably transformed with LiveDrop-GFP. In control cells cultured in +Oleate conditions, Pex14 localized to both punctate spots indicating peroxisomes and colocalizes with LiveDrop (Fig. 7A; Fig. S6A). Pex16 initially recruits Pex3 to the ER or to existing peroxisomes (Aranovich et al., 2014; Matsuzaki and Fujiki, 2008). Pex3 then serves as the docking module for the cytosolic chaperone, Pex19, to import PMPs including Pex14 (Fang et al., 2004). In *Pex3*i cells, fewer Pex14 punctate spots were observed, as PMP insertion would be suppressed, and the colocalization of Pex14 with LiveDrop was enhanced (Fig. 7B; Fig. S6B). Similarly, in *Pex16*i or *Pex19*i cells, colocalization of Pex14 with LiveDrop was enhanced, and the number of punctate Pex14 spots in the peroxisome characteristic pattern was suppressed (Fig. 7C,D; Fig. S6C,D). Pex13 is thought to interact directly with Pex14 to help its trafficking to peroxisomes and to form the docking complex for importing proteins such as peroxisomal enzymes (Itoh and Fujiki, 2006; Matsuzaki and Fujiki, 2008). Reduced punctate Pex14 spots were observed in *Pex13*i cells, but colocalization of Pex14 with LiveDrop was enhanced (Fig. 7E; Fig. S6E). In *Pex1*i cells, a similar pattern of punctate spots was observed relative to control, but they were smaller in size (Fig. 7F; Fig. S6F), as Pex1 functions after PMP insertion to recycle Pex5 and promote enzyme import through the Pex14 docking complex (Fujiki et al., 2020). There was no noticeable enhancement of Pex14 localization to the LD surface in *Pex1*i cells (Fig. 7F; Fig. S6F). Pex5 interacts directly with Pex14 to import peroxisome enzymes through the docking complex (Gaussmann et al., 2021). In *Pex5*i cells, fewer punctate Pex14 spots were present but there was no enhancement of Pex14 colocalization with LiveDrop (Fig. 7G; Fig. S6G). In *Pex14*i cells, few Pex14 punctate spots were observed and little colocalization with LiveDrop was observed (Fig. 7H; Fig. S6H). Only *Pex3*i, *Pex13*i, *Pex16*i and *Pex19*i caused significant increases in the proportion of Pex14 surrounding LDs (Fig. 7I). This is notable as Pex3, Pex16 and Pex19 are the Pex proteins needed to insert PMPs like Pex14, and likely Pex13, into the peroxisome membrane (Fujiki et al., 2020).

A subset of *Pex*i was tested in *Pex19*KO cells under lipolytic conditions to examine peroxisome-independent functions of each Pex gene in lipid storage. *Pex1*i and *Pex3*i had little effect on the volume or number of LDs in cells cultured in lipolytic conditions (Fig. 7J–O; Fig. S6I). *Pex5*i reduced the volume of LDs but increased their average number, suggesting increased fragmentation (Fig. S6I). *Pex13*i or *Pex14*i caused significantly reduced total LD volume in lipolytic cells (P<0.001, Fig. 7P; Fig. S6I).

Pex3 and Pex13 colocalize with peroxisomes and the LD surface

Very few peroxisomes (punctate SKL) overlap LDs (LiveDrop) in S2 cells cultured in +Oleate conditions (Fig. 8A). Transient transfection of transgenes expressing HA-tagged Pex proteins was used to determine whether Pex proteins other than Pex14 were also associated with LDs. HA-Pex1 was largely cytoplasmic, but a proportion of HA-Pex1 was concentrated at peroxisomes (Fig. 8B). Overexpressed HA-Pex3 suppressed peroxisome formation. HA-Pex3 formed a reticular pattern surrounding the nucleus as well as surrounding, but not overlapping, LiveDrop-GFP (asterisks) and was also concentrated at the few remaining peroxisomes (Fig. 8C). HA-Pex5 was also homogenous throughout the cytoplasm as expected by its function, but again a significant proportion was concentrated at peroxisomes. However, no colocalization with LiveDrop was ever observed (Fig. 8D). HA-Pex10, which together with Pex2 and Pex12 forms a E3 ligase complex needed to traffic Pex5 back out of the peroxisome (Fujiki et al., 2020), strongly overlapped with peroxisomes but did not appreciably colocalize with LiveDrop (Fig. 8E). Two distinct phenotypes were observed with overexpression of HA-Pex13. In cells in which transgene expression was relatively lower (Fig. 8F, right-most cell), HA-Pex13 overlapped with peroxisomes. However, when HA-Pex13 levels were relatively higher, fewer peroxisomes were observed and the majority of HA-Pex13 overlapped the LiveDrop signal (Fig. 8F, second left, asterisk). Finally, HA-Pex16 cells had a reduced number of peroxisomes compared to control cells (Fig. 8A) and the HA-Pex16 signal did not overlap with LiveDrop (Fig. 8G). HA-Pex19 cells also had a similar number of peroxisomes to control cells, but they were often larger (Fig. 8H). HA-Pex19 also did not show observable colocalization with LiveDrop (Fig. 8H).

Recruitment of Pex14 to LDs is observed in mammalian NRK cells

The recruitment of Pex14 to LDs independently of mature peroxisomes was conserved in mammalian cells. When NRK cells were cultured in standard conditions, the PEX14 signal overlapped peroxisomes (Fig. 8I). When cultured in +Oleate conditions (1 mM oleic acid for 48 h), a portion of the PEX14 distinct from ABCD3 surrounded LDs (Fig. 8J). The proportion of PEX14 adjacent to LDs increased significantly from 4.7% in standard conditions to 32.8% in +Oleate conditions (Fig. 8K). However, the proportion of mature peroxisomes adjacent to LDs was largely the same in standard or +Oleate conditions (Fig. 8L). Like what was observed in S2 cells, no change in NRK cell peroxisome volume was observed in +Oleate conditions (Fig. 8M), but peroxisome number increased significantly (P<0.01, Fig. 8N). Corresponding to what was seen in +Oleate cultured S2 cells (Fig. 2D), PEX14 levels were relatively higher in NRK cells cultured in +Oleate at 24 h and remained higher even after 48 h (Fig. 8O).

Journal of Cell Science (2022) 135, jcs259092. doi:10.1242/jcs.259092

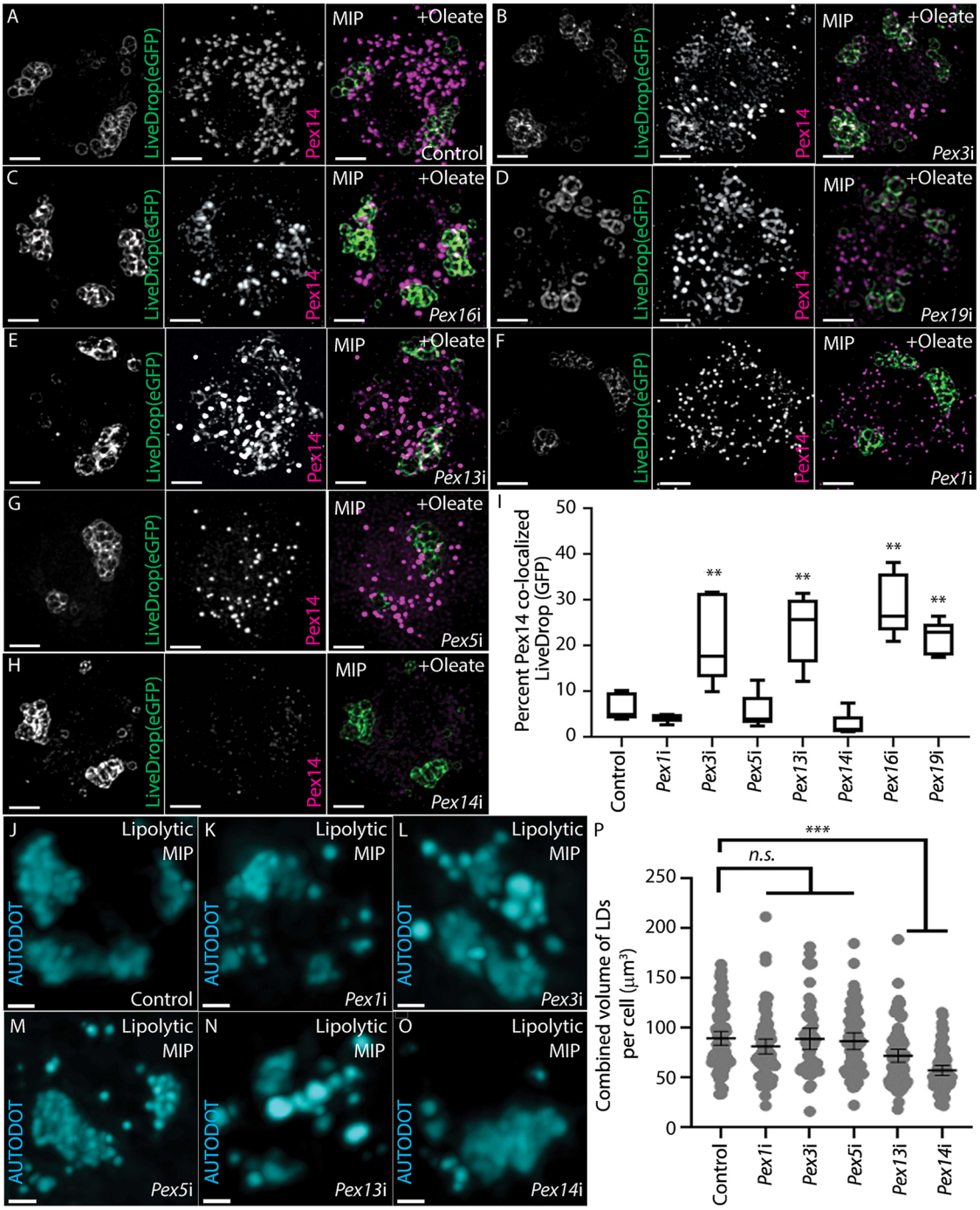

Fig. 7. Knockdown of Pex genes involved in early peroxisomal biogenesis pathway and Pex14 transport enhances Pex14 localization to the LD surface. (A) In S2 cells stably transfected with LiveDrop-GFP, the pattern of Pex14 is punctate dots (peroxisomes) colocalized with LiveDrop. (B–E) *Pex3*i (B), *Pex16*i (C), *Pex19*i (D) and *Pex13*i (E) cells all had relatively fewer punctate Pex14 spots compared to controls, and all showed enhanced Pex14 colocalization with LiveDrop. (F) *Pex1*i cells had smaller and relatively more peroxisomal Pex14 punctate spots and less Pex14 colocalization with LiveDrop. (G) *Pex5*i cells had relatively fewer Pex14 punctate but Pex14 colocalization with LiveDrop was not enhanced. (H) *Pex14*i cells had very little Pex14 signal. Single-plane images for each MIP image are shown in Fig. S6. (I) *Pex3*i, *Pex13*i, *Pex16*i and *Pex19*i cells had relatively higher colocalization of Pex14 with LiveDrop (**P<0.01; Mann-Whitney test), whereas other *Pex*i cells did not show a significant difference. The box represents the 25-75th percentiles, and the median is indicated. The whiskers show the 5-95th percentiles. (J–O) Live imaging of AUTODOT-labeled LDs in *Pex*i-treated *Pex19*KO S2R+ cells grown in lipolytic conditions. Control (J), *Pex1*i (K), *Pex3*i (L) or *Pex5*i (M) all had similar LD volumes. (N,O) *Pex13*i (N) or *Pex14*i (O) cells had reduced total LD volume. (P) Total LD volume (μm^3) of *Pex*i dsRNA-treated cells in lipolytic condition showed that only *Pex13*i and *Pex14*i had significant reduction in LDs (mean±95% c.i.; ***P<0.001, Mann–Whitney test). Scale bars: 2 μm. n.s., not significant.

DISCUSSION

Here, in *Drosophila*, we identified lipid-responsive LD association of a subset of Pex proteins (Pex3, Pex13 and Pex14) that were not part of mature peroxisomes. When associated with LDs, Pex14 affected recruitment of Hsl and influenced TG storage and mobilization of TGs (Fig. 5C,D). Although Pex13 overexpression affected Hsl recruitment to LDs, the effect was more muted (Fig. S5C,D). Thus, our data favor a model whereby Pex14 plays a

Journal of Cell Science (2022) 135, jcs259092. doi:10.1242/jcs.259092

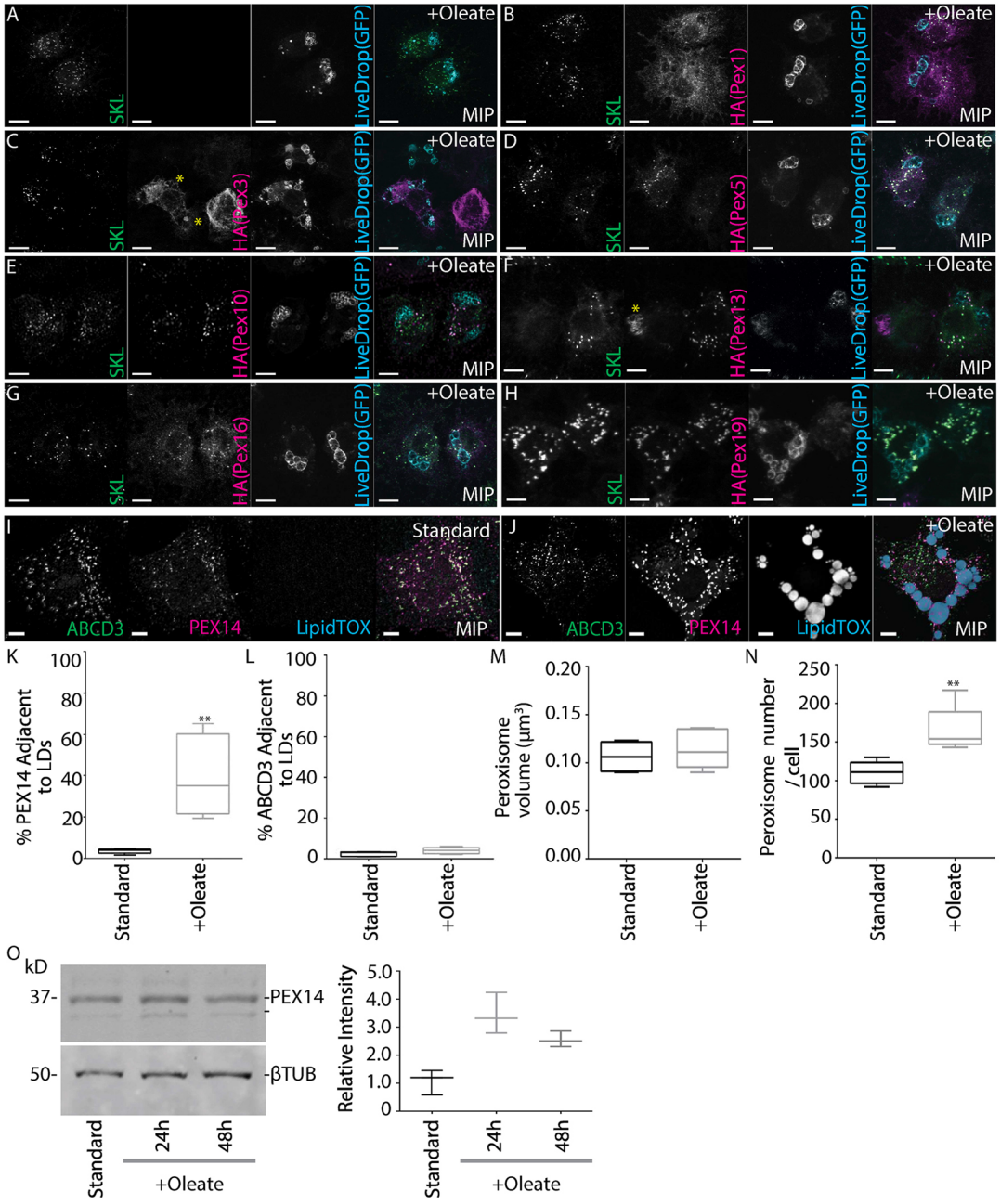

Fig. 8. Pex3 and Pex13, but not other Peroxins, colocalize with the LD surface independently from peroxisomes in S2 cells cultured with oleic acid. (A) Cells stably expressing LiveDrop-GFP. (B) HA-Pex1 was cytosolic with some proportion at peroxisomes (SKL). Overlap with LiveDrop was not observed (C) HA-Pex3 formed a reticular pattern throughout the cell; some signal overlapped with LiveDrop. Many cells also displayed reduced numbers of peroxisomes. Asterisk indicates areas of the cell where HA and LiveDrop signals overlap. (D) HA-Pex5 colocalized with peroxisomes and was diffuse in the cytosol. No colocalization was seen with LiveDrop. (E) HA-Pex10 overlapped with peroxisomes but not LiveDrop. (F) Cells with relatively lower HA-Pex13 signal (right-most cell) showed it localizing to peroxisomes while cells with relatively higher HA-Pex13 signal (left-most cell) had a reduced number of peroxisomes and HA-Pex13 had a high degree of LiveDrop colocalization. Asterisk indicates areas of the cell where HA and LiveDrop signals overlap. (G) HA-Pex16 overlapped with a reduced number of peroxisomes but not LiveDrop. (H) HA-Pex19 colocalized with peroxisomes (SKL) but not with LiveDrop. The relative increase in size of the punctate SKL signal suggests that peroxisomes were enlarged. (I) In standard cultured NRK cells, the peroxisome marker ATP-binding cassette subfamily D member 3 (ABCD3) signal colocalized with PEX14. (J) In +Oleate cultured cells, PEX14 surrounded LDs (LipidTox) independently of ABCD3. Images are MIPs of an entire cell. (K) The proportion of PEX14 adjacent to LDs (LipidTOX) increased significantly in +Oleate culture (**P<0.01; unpaired two-tailed Student's t-test). (L) The proportion of ABCD3 adjacent to LDs was similar when cells were cultured in +Oleate or standard conditions. (M) Peroxisome volume was similar in standard or +Oleate cultured NRK cells. (N) The number of peroxisomes increased in +Oleate NRK cells (**P<0.01; unpaired two-tailed Student's t-test). For box plots in K-N, the box represents the 25-75th percentiles, and the median is indicated. The whiskers show the 5-95th percentiles. (O) After transfer to +Oleate conditions, the level of PEX14 increased at 24 h and remained high at 48 h (mean±s.d.). Scale bars: 1 µm (A–H) and 2 µm (I,J).

more active role in LD regulation that is functionally and/or temporally distinct from previously characterized roles for Pex14 in peroxisome biogenesis or movement (Bharti et al., 2011; Gaussmann et al., 2021; Reuter et al., 2021). When *Pex14*i +Oleate cultured cells were transferred to lipolytic conditions, LD fragmentation occurred (Fig. 3A–D,G,H). Further supporting a role

Journal of Cell Science (2022) 135, jcs259092. doi:10.1242/jcs.259092

for Pex14 in promoting TG storage, the LDs in cells overexpressing both Pex14 and Hsl were significantly larger and less numerous than those in cells overexpressing Hsl alone (Fig. 5G,H). The *Drosophila* DGAT homolog, *Diacylglycerol O-acyltransferase 2* (*Dgat2*), acts in opposition to LD lipolysis (Wilfling et al., 2013). However, RNASeq indicated that *Dgat2* mRNA was absent from S2 cells in all conditions. The relative increase in TG lipolysis (free glycerol) levels in *Pex14*i lipolytic cells compared to control (Fig. 3I) supports a model in which Pex14 also suppresses lipase activity at LDs. This model is also supported by observations that LD volume in the fat body and overall TG content is significantly reduced by *Pex14*i in the larval fat body (Fig. 1E).

The mechanism underlying non-peroxisomal retention of Pex14 at LDs is suggested by *Pex19*KO cells (Fig. 7P). *Pex19*KO or *Pex19*i cells had a marked increase in Pex14 surrounding LDs in +Oleate cultured cells (Fig. 4A,B and Fig. 7D). *Drosophila Pex19* mutants have elevated activity of cytoplasmic (non-LD-associated) lipases, causing mitochondrial dysfunction and lipotoxicity (Bülow et al., 2018). Given that Pex19 directs Pex14 to the peroxisome membrane, loss of Pex19 would promote association of Pex14 with LDs, which could also contribute to disruption of lipid metabolism. This could also explain enhancement of Pex14 LD recruitment by *Pex*3i, *Pex13*i and *Pex16*i (Fig. 7B,C,E). The targeting of Pex14 to a peroxisomal membrane requires Pex3, Pex16 and Pex19 (Fujiki et al., 2020). Pex13 also assists insertion of Pex14 into the peroxisome membrane (Itoh and Fujiki, 2006). Enhanced localization of Pex14 to the LD surface in *Pex3*i, *Pex13*i, *Pex16*i or *Pex19*i cells strongly suggests that Pex14 association with LDs is not part of canonical peroxisomal protein import (Fig. 7A–E; Fig. S6A–E). Notably, Pex14 trafficking to the LDs was not affected by *Pex*i of genes needed for later stages of peroxisome biogenesis like *Pex1* or *Pex5* (Fig. 7F,G; Fig. S6F,G). In *Pex3*-deficient yeast, Pex14 is trafficked to the ER via the Sec61 translocon, which was also shown recently to assist in translocation of LD proteins to the ER *in vitro* (Leznicki et al., 2022; van der Zand et al., 2010).

The targeting of Pex14 to peroxisomes relies on successful binding to the cytosolic chaperone, Pex19, via its N-terminal Pex14 domain (Itoh and Fujiki, 2006; Neufeld et al., 2009). In *Pex19*-deficient cells, Pex14 accumulates at the ER and at mitochondria in yeast and mammals, respectively (Sacksteder et al., 2000; van der Zand et al., 2010). It has been proposed that Pex14 can be inserted into mitochondrial membranes (Sugiura et al., 2017). In *Pex19*KO cells, we found that all LD-associated Pex14 signal was distinct from mitochondria (Fig. 4B), while some signals were in close proximity to the ER (Fig. 4A). Super-resolution imaging showed that Pex14 surrounding LDs is not entirely associated with ER (Fig. 4D). This is different from other proteins identified previously to mediate peroxisome LD-association, such as FAF2 (also known as UBXD8) (Schrul and Kopito, 2016).

Blocking peroxisome Class I and II PMP bilayer membrane insertion pathways via *Pex19*KO, *Pex3*i, *Pex16*i or *Pex19*i increased the relative Pex14 association with LDs (Fig. 4A,B and Fig. 7B–D), suggesting that Pex14 at LDs is not part of a PPV or peroxisome bilayer membrane. Mutant forms of PEX14 in which the TM domain was non-functional did not localize to any membranes in Chinese hamster ovary cells (Itoh and Fujiki, 2006). Similarly, although the TM domain is sufficient to associate Pex14 with the LD surface (Fig. 6), the Pex14 domain that mediates formation of the docking complex is not, consistent with enhanced Pex14 localization observed in *Pex19*KO/*Pex19*i cells (Fig. 4A-C and Fig. 7D).

Insertion of Pex14 into the peroxisome membrane to form the docking complex creates large pores through which folded proteins can be imported by Pex5 (Azevedo and Schliebs, 2006; Will et al., 1999). This likely occurs in partnership with Pex13 (Otera et al., 2002). Thus, the TM domain of Pex14 faces hydrophilic and hydrophobic environments and has an amphipathic helix conformation. This same amphipathic property of the Pex14 TM domain (Fig. S7) might insert into the LD monolayer membrane. This would account for the alkaline carbonate-resistant retention of Pex14 in fractionated LDs (Fig. 2I). Co-overexpression of Pex14 and Hsl shows that the C-terminal region of Pex14 can inhibit Hsl-mediated LD fragmentation (Fig. 6K–M). However, the C-terminal half of Pex14 is poorly characterized. There is a coiled-coil domain (CCD) near the TM domain sufficient for homodimerization/oligomerization and subsequent interaction with Pex13 (Itoh and Fujiki, 2006). The CCD is predicted within the C-terminal end (aa159–209) of Pex14 (Ludwiczak et al., 2019). The role for this CCD or dimerization/oligomerization of *Drosophila* Pex14, or interaction of Pex14 with Pex13 at LDs, remains to be determined. PEX14–PEX5 interaction is required to regulate peroxisome–LD interactions and ATGL recruitment during fasting-induced lipolysis at LDs (Kong et al., 2020). Retention of Pex14 at the LD surface may play a role in priming such events.

Whether Pex14 requires the canonical partner Pex13 remains to be investigated. Pex3 is likely to have a separate role at the LDs from Pex13 and Pex14 because FAF2, trafficked to LDs via the action of Pex3 and Pex19, inhibits the action of ATGL (Olzmann and Carvalho, 2019; Schrul and Kopito, 2016). This provides explanation for the sensitivity of *Pex3*i larvae in lipid-reduced condition (Fig. 1E) and less pronounced LD fragmentation in *Pex19*KO *Pex3*i cells under lipolytic condition (Fig. 7P; Fig. S6I). Both *Pex13*i larvae (Fig. 1E) and *Pex19*KO *Pex13*i cells (Fig. 7P) suggest that Pex13 confers a similar, but less pronounced, function to Pex14 at the LD surface. Co-overexpression of Hsl and Pex13 in lipolytic condition suppressed LD fragmentation like Pex14 (Fig. 5C,D; Fig. S5C,D). Therefore, Pex13 may assist Pex14 in mitigating Hsl-mediated lipolysis without contributing to its trafficking to the LD surface (Fig. 7E). Supporting the model that Pex14 and Pex13 work together at the LD surface is the observation that changes in the amount of PLIN affects LD localization of Pex14 and Pex13 (Fig. 5J,N). Overexpression of *Lsd-1* suppressed the localization of Pex13 and Pex14 to the LD surface (Fig. 5J,N), but elevated Lsd-2 levels did not affect Pex14 association with LDs (Fig. 5I).

A major mechanism regulating protein association with the LD surface is inter-molecular competition for limited space as the LD grows and shrinks (Kory et al., 2015). As the LD surface shrinks during TG lipolysis, proteins lose association from the LD surface, creating space for lipases (Kory et al., 2015). Exclusion of Pex14 from LDs when Lsd-1 levels are elevated (Fig. 5L) suggests that this is occurring. As overexpression of *Lsd-2* does not affect Pex14-LD localization, the effect of *Lsd-1* overexpression on Pex14 is likely a specific, rather than general, effect. The major circulating neutral lipid in *Drosophila* is DG, which is accumulated in the fat body for energy storage (Heier and Kühnlein, 2018). Although Pex14 levels at the LD have little effect on the TG lipase Bmm, Pex14 antagonizes Hsl at the LD (Fig. 5A–H). This supports a model whereby recruitment of Pex14 to the LD surface perturbs the interaction between Hsl and Lsd-1, blocking the recruitment of Hsl to the LD, with the antagonistic effects of overexpression of *Lsd-1* on Pex14-LD localization (Fig. 5J). Further studies are required to determine the molecular mechanism by which Pex14 suppresses Hsl recruitment to LDs.

Given the absence of peroxisome proliferation observed in S2 cells transferred to +Oleate conditions, it is likely that newly synthesized Pex13 and Pex14 directly associate with LDs. A local pool of proteins associated with the LD surface needed to form the peroxisome docking complex could couple local peroxisome assembly to TG lipolysis. However, this model, including any Pex14-dependent or -independent role for Pex3 and Pex13 recruitment to LDs, needs to be addressed experimentally.

MATERIALS AND METHODS

Cell culture

S2 and S2R+ *Pex19*KO cells were obtained from the *Drosophila* Genomics Resource Centre. Cell identity was validated by RNASeq and lack of contamination tested by visual observation or qRTPCR as needed. 'Standard' conditions for culturing S2 and S2R+ cells were Schneider's medium (Sigma-Aldrich S0146) containing 10% fetal bovine serum (FBS; Thermo Fisher 12483-012) at 25°C. The standard culture conditions for NRK cells were Dulbecco's modified Eagle medium (Sigma-Aldrich D5796) containing 10% FBS at 37°C and 5% CO_2. The +Oleate culture conditions used in this study are the same as used previously to induce LDs in S2 cells (Guo et al., 2008; Kramer et al., 2018), where standard medium was supplemented with 1 mM oleic acid (+Oleate, Sigma-Aldrich O1008) bound to fatty acid-free bovine serum albumin (BSA; Sigma-Aldrich A8806). Cells were maintained in +Oleate conditions for 24 h to 48 h. To induce LD lipolysis, S2 cells cultured in +Oleate conditions for 24 h cells were washed 1× in fresh Schneider's medium and transferred to Schneider's medium without FBS or oleic acid supplementation for 24 h (Guo et al., 2008). All culture media were supplemented with 100 U penicillin/ml and 100 µg streptomycin/ml (Thermo Fisher 15140-122). S2, S2R+ and NRK cells were passaged at log phase before they reached confluency. Cultures were not used beyond passage 25.

Generation of polyclonal antiserum recognizing *Drosophila* Pex14

The full-length Pex14 open reading frame (Baron et al., 2016) cloned into PENTR-D (Thermo Fisher) was transferred to pDEST-17 (Thermo Fisher) using LR ClonaseII (Thermo Fisher 11791-020) and expressed in BL21-AI *Escherichia coli* (Thermo Fisher C6070-03) grown to an OD_{600} of 0.4 at 37°C with shaking by addition of 0.2% L-arabinose and then cultured at 25°C for 3 h. Bacterial cell pellets were lysed by incubation in 8 M urea, and cleared by centrifugation at 20,000 ***g*** for 30 min at 25°C. The cleared lysate was applied to a 1 ml HisTrap column (Cytavia 17524701), using the Akta-Start His-tagged purification protocol (Cytavia). Purified protein was eluted using a stepwise imidazole gradient. Fractions containing purified Pex14 were combined, transferred to dialysis tubing (8000 MWCO, Spectrum 132660) and desalted by buffer exchange in 5 l 1× PBS overnight. Purified protein was concentrated in an Amicon Ultra 15 centrifugal filter (Millipore-Sigma UFC900308) to 1 mg/ml and injected into guinea pigs (Pocono Rabbit Farms and Laboratories). The partially purified serum was validated for antigen specificity by western blotting against purified bacterially expressed Pex14 as well as lysates from S2 cells, S2 cells expressing Pex14-GFP fusions and *Pex14*i S2 cells, confirming the presence or absence of a single band of expected size.

Drosophila strains

The w^{1118} strain was obtained from the Bloomington *Drosophila* Stock Center (BDSC). All crosses were performed at 25°C. TRiP UAS-RNAi transgenes against Pex genes were obtained from the BDSC. These included the following: *Pex1*i BDSC:28979 (y^1 v^1; P{$y^{+t7.7}$ $v^{+t1.8}$=TRiP.HM05190}attP2); *Pex1*i BDSC:51497 (y^1 v^1; P{$y^{+t7.7}$ $v^{+t1.8}$=TRiP.HMC03252}attP2); *Pex5*i BDSC:55322 (y^1 v^1; P{$y^{+t7.7}$ $v^{+t1.8}$=TRiP.HMC04009}attP40); *Pex14*i BDSC:77180 (y^1 v^1; P{$y^{+t7.7}$ $v^{+t1.8}$=TRiP.HMC06491}attP40); and *Pex16*i BDSC:57495 (y^1 *sc** v^1 sev^{21}; P{TRiP.HMC04810}attP2). Additional UAS-RNAi transgenic stocks targeting Pex genes were obtained from the Vienna *Drosophila* Resource Center (VDRC). These included the following: *Pex2*i VDRC:108578 KK; *Pex3*i VDRC:11017 GD; *Pex10 VDRC*:110405 KK; *Pex11ab*i VDRC:105654 KK; *Pex12*i VDRC:34671 GD; *Pex13*i VDRC:39544 GD; *Pex14*i VDRC:42590 GD; *Pex16*i VDRC:34296 GD; *Pex19*i VDRC:100746 KK; and *Pex19*i VDRC:22064 GD. Driver lines used were as follows: y^1, *w**, UAS-*Dicer*; P{w^{+mC}=r4-GAL4}3; y^1, *w**, UAS-*Dicer*; P{*TubP*-GAL4}LL7/*TM3*(Ubi-GFP), Sb^1 (Kyoto *Drosophila* Stock Center 108069). Fly stocks were maintained on the BDSC standard cornmeal food recipe and passaged once a week to prevent overcrowding. To obtain second-instar larvae for feeding assays, flies of each genotype were transferred to bottles with food for 24 h. After 3 days, the food was scraped from the bottle and rinsed with distilled water to expose larvae. The developmental stage was confirmed by the characteristic shape of the larval mouth hooks.

Cloning

Myc-, HA- or FLAG-tagged Pex vectors were described previously (Baron et al., 2016). Pex14 truncations were generated by PCR into the pENTR/D Gateway entry vector by TOPO cloning (Thermo Fisher K240020) and recombined into pARW or pAWR using LR ClonaseII. To generate LiveDrop (Wang et al., 2016), DNA encoding aa160–216 of *Drosophila Glycerol-3-phosphate acyltransferase 4* (*Gpat4*) was cloned via PCR into pENTR/D and recombined into pAWR or pAWG vectors. Plasmids were transfected into *Drosophila* S2 cells using Effectene transfection reagent (Qiagen 301425). S2 cells were passaged 24 h before transfection. Approximately 5.0×10^5 cells were transfected with 150 ng plasmid DNA. Transfected S2 cells were incubated at 25°C for 48–72 h before fixation for imaging. Clonal populations of stably transfected LiveDrop GFP S2 cells were selected by fluorescence-activated cell sorting (Faculty of Medicine and Dentistry Flow Cytometry Facility, University of Alberta) followed by limiting serial dilution in conditioned Schneider's medium in 96-well plates (Luhur et al., 2019).

^{35}S metabolic pulse-chase labeling

To label newly synthesized protein in S2 cells, Schneider's medium (Schneider, 1972) without L-methionine, L-Cysteine or yeast extract was supplemented with 10% dialyzed FBS (Thermo Fisher A33820) and 100 µl Easy Tag Express ^{35}S Methionine/Cysteine (Perkin Elmer NEG 772002MC) at either 0 h or 24 h after transformation with a 6xMyc-Pex14 (pAMW-Pex14) as described above. Twenty-four hours after transformation, 1 mM oleic acid was added. Cells in which ^{35}S was added at 0 h were washed in complete Schneider's medium (Schneider, 1972) at 24 h. Cells in which ^{35}S Methionine/Cysteine mix was added at 24 h were washed in Schneider's medium at 72 h. The cells were pelleted at 72 h and rinsed with PBS containing cOmplete Protease Inhibitor (Millipore 04693159001) and the LDs selectively fractionated as described below. The presence of radiolabeled 6xMycPex14 was analyzed by immunoprecipitation from each fraction and detected by autoradiography.

Imaging

Fixed S2 cells were observed using a Zeiss 63× oil immersion objective (1.4 NA) on a Zeiss Axio Observer M1 microscope with an ERS spinning disk confocal and a C9100 EMCCD camera (Hamamatsu) using Volocity imaging software (PerkinElmer) or a Zeiss LSM700 confocal and Zen 2009 software (Zeiss). Live S2 cells suspended in Schneider's medium were observed using a C-Apochromat 63×/1.2 W Corr (0.14–0.19 mm) objective. Super-resolution imaging was performed using a Leica Plan Apochromat 100× oil immersion (1.4 NA) objective on a Falcon SP8 STED. The depletion lasers were set to provide 30 nm lateral resolution. Image stacks were captured at 130 µm vertical (*z*) spacing (ERS) or 10 to 25 nm (LSM700).

Cell and tissue fixation

Cells were grown in six-well dishes containing a #1.5 cover glass coated with concanavalin A (Millipore-Sigma; Rogers et al., 2002). Cells were fixed for 10–20 min in 4% paraformaldehyde in PBS (Baron et al., 2016). Fat bodies were hand dissected from third-instar larvae and fixed for 60 min in 4% paraformaldehyde dissolved in PBS. Following fixation, cells or tissues were incubated in blocking solution (4% BSA in PBS) and then for 1 h or overnight in primary antibody in blocking solution. For Pex14, CytC

and Cnx99A primary antibodies, 0.1% Tween-20 was used instead of 4% BSA in the blocking solution. Primary antibodies included monoclonal mouse anti-FLAG M2 (1:200, Sigma-Aldrich F3165), rabbit anti-Myc (1:200, Sigma-Aldrich SAB4301136), monoclonal mouse anti-Myc (1:250, 9B11, Cell Signaling Technology 2276S), monoclonal rat anti-HA (1:2000, Millipore-Sigma 3F10), guinea pig anti-Pex14 (1:1000), rabbit anti-Abcd3 primary antibody (1:500) (Huang et al., 2020), mouse anti-Cytochrome C (1:500, BD Pharmingen 7H8.2C12), mouse anti-Cnx99A (6-2-1, S. Munro, Developmental Studies Hybridoma Bank) and rabbit anti-SKL antibody (1:200, R. Rachubinski, University of Alberta). Primary incubation was followed by washing 3×20 min in block solution followed by incubation with donkey anti-mouse AlexaFluor 568 (Life Technologies A10037), donkey anti-mouse AlexaFluor 647 (Invitrogen A31571), donkey anti-guinea pig Cy3 (Jackson ImmunoResearch 706-165-148), donkey anti-guinea pig 647 (Jackson ImmunoResearch 706-606-148), donkey anti-rat A568 (Abcam ab175476), donkey anti-rabbit AlexaFluor 488 (Invitrogen A21206), or donkey anti-rabbit 647 (Abcam ab150067), all at 1:2000 dilution. To detect LDs, fixed cells or tissues were incubated with LipidTOX Deep Red (647 nm, Thermo Fisher) or AUTODOT (405 nm Monodansylpentane, Abcepta) at 1:500 dilution for 1 h after secondary antibody incubation, while live cells were incubated in AUTODOT for 30 min prior to imaging. Cells and tissue were mounted in ProLong Gold mounting medium (Thermo Fisher P36930).

NRK cells were fixed in 4% paraformaldehyde and blocked in 3% BSA for 1 h, incubated in rabbit anti-PEX14 (Thermo Fisher PA5-78103) and mouse anti-ABCD3 (R. Rachubinski, University of Alberta) at 1:200 dilution, for 1 h. Primary antibody incubation was followed by 3× washes in blocking solution followed by incubation with goat AlexaFluor 568 anti-mouse or AlexaFluor 488 anti-rabbit (1:2500, Abcam ab175473 and ab150077, respectively).

Image processing and quantification

Image stacks of individual images sampled at sub-Nyquist Z-resolution comprising the entire cell volume were deconvolved by Classical Maximum Likelihood Estimation (confocal) algorithm in Huygens Professional Software (Scientific Volume Imaging) using an experimentally determined point spread function constructed from multiple images of 0.1 µm Tetraspeck beads (Thermo Fisher T7279). Three-dimensional colocalization analysis was performed using Huygens Professional Software (Scientific Volume Imaging) using Pearson's coefficient (Adler and Parmryd, 2010). Average peroxisome or LD volume and number per cell were calculated using IMARIS software v9 (Oxford Instruments). To validate our estimation of background fluorescence colocalization, measurements were also calculated on images in which one channel was shifted 90°, relative to the other (Dunn et al., 2011). In all cases, measured background colocalization was less than 10%. The proportion of signal surrounding LipidTOX or AUTODOT marked LDs (% Adjacent) was performed using a modified method used previously for signal adjacent to peroxisomes (Dahan et al., 2022). Briefly, a surface corresponding to each LD signal above the local background was generated encompassing the LD volume using the 'Surfaces' function. This volume was expanded by 6 voxels, and the signal within inner shell subtracted from the outer shell and reported as a percentage of total signal within the cell. All quantifications were based on at least three independent biological replicates with five or more cells in each replicate. Unless stated otherwise, colocalization significance and organelle volume/number data were assayed using an unpaired two-tailed Student's *t*-test.

dsRNA production and RNAi knockdown conditions

A prevalidated template library (Foley and O'Farrell, 2004) was used to generate dsRNA using T7 RNA Polymerase (Thermo Fisher EP0111) or a HiScribe T7 High Yield RNA Synthesis Kit (New England BioLabs E2040S). S2 cells were passaged 24 h prior to dsRNA treatments. Effectene Transfection Reagent (Qiagen 301425) was used to enhance dsRNA uptake. Cells were incubated with ∼15 µg dsRNA for 4 days (reapplied after 48 h) and subsequently incubated in 1 mM oleic acid containing media free of dsRNA for 24 h. A scrambled dsRNA amplicon was used as a control (forward primer sequence, 5′-GTGAAGAGGTCAGAGGCCTG-3′; reverse primer sequence, 5′-ACAGTCTAGCGTTCCTTGAGG-3′).

qRTPCR analysis

RNA was isolated from S2 cells or from larvae using the RNeasy Plus Mini Kit (Qiagen 74134) and reverse transcribed using the Maxima H minus system (Thermo Fisher K1681). Quantification was performed using Perfecta SYBR Green FastMix (QuantaBio 95118) and an Eppendorf MasterCycler RealPlex2. All samples were measured in triplicate and calculations were made relative to *Ribosomal protein L30* (*RpL30*) expression. Primers used for each of the target genes were experimentally validated pairs reported in FlyPrimerBank (Hu et al., 2013). For all qRTPCR experiments, values reported are averages based on three biological replicates. Statistical significance was determined by unpaired Student's *t*-test or one-way ANOVA.

RNASeq and analysis

Three independent replicates of S2 cells cultured in Schneider's medium (starved), Schneider's+FBS (standard) or Schneider's plus oleic acid (+Oleate) culture conditions were compared. A replicate of starved cells was also treated with 3AT (Samis et al., 1972). Total RNA was isolated from each using the RNeasy Plus Mini Kit. RNA integrity was verified using an Agilent RNA Nano assay (Agilent Genomics 5067-1511). Ribosomal RNA was subtracted from samples using a Ribo-Zero Gold rRNA Removal Kit (Illumina 20040526). Libraries were prepared using a NEBNext Ultra RNA Library Prep Kit and NEBNext Multiplex Oligos (New England Biolabs E7530L and E7335L). Library quality and size distribution were confirmed by running an Agilent High Sensitivity DNA assay (Agilent Genomics 5067-4626), and the average size of library inserts was verified to be 290–300 bp. Then, 10 pM of each of the libraries was loaded onto an Illumina MiSeq v2 300 cycle kit (2×150 cycles, paired-end reads, MS-102-2003). Paired-end reads were aligned to the *Drosophila melanogaster* genome (6.28 release) using HiSat2 (Kim et al., 2015). Individual read counts were mapped to specific genes using HTSeq (Anders et al., 2015). Reads with less than one count per million in at least three samples were filtered. Differential analysis was performed using the SARTools pipeline (version 1.74) pipeline (Varet et al., 2016) that evaluates differential mRNA levels using both EdgeR (Robinson et al., 2010) and DESeq2 (Love et al., 2014) algorithms. Transcripts with significantly differential expression ($P<0.05$, $P\text{adj}<0.1$) were considered for subsequent analysis. Gene set enrichment analysis (GSEA) was performed on both the EdgeR and DESeq datasets using EasyGSEA, which is part of the easy Visualization and Inference Toolbox for Transcriptome Analysis (eVITTA) toolbox (version 1.31) (Cheng et al., 2021). RNASeq datasets were deposited in the NCBI BioProject database (PRJNA807290).

Larval lipid storage (flotation) assay

Ten y^1, *w**, UAS-Dcr; r4-GAL4 females were crossed to ten UAS-*Pex*i males and placed in a vial with fresh BDSC food and raised at constant 25°C. After 3–4 days, late third-instar larvae were isolated, rejecting larvae that had begun to pupariate (everted spiracles). Larvae were transferred to a 1 ml clear plastic cuvette containing 1 ml solution of 16% sucrose (w/v) dissolved in PBS (Reis et al., 2010). Images were captured of each replicate compared to a corresponding y^1, *w**, UAS-Dcr; r4-GAL4 x w^{1118} control. Using ImageJ, images of each replicate were analyzed by drawing a line from the base of the cuvette to the center of the liquid meniscus. The positions of larvae relative to the cuvette base were then measured and their vertical position expressed as a fraction relative to the distance to the meniscus. Combined measurements for three biological replicates of each genotype were analyzed using SuperPlotsofData (Goedhart, 2021). Statistical significance relative to the control for each genotype was measured by an unpaired Welch's *t*-test.

TG/glycerol quantification

Third-instar larvae were rinsed in sterile PBS and homogenized in 5% NP-40 in distilled, deionized water. Samples were heated at 80°C for 5 min, cooled to room temperature and centrifuged to remove insoluble material. TG measurements were made using a Triglyceride Assay Kit (Abcam

ab65336), measured on a BioTek Synergy 4 plate reader with Gen 5 software. TG measurements were normalized to the protein concentration of each sample, measured using a Pierce BCA Protein Assay Kit (Thermo Fisher 23225). Ten larvae for each trial were tested and reported as averages from three biological replicates. Statistical significance was measured by unpaired Student's *t*-test.

TG lipolysis was quantified using a Glycerol Assay Kit (Sigma-Aldrich MAK117). S2 cells were pelleted by centrifugation and the pellet diluted 1:1000 in water. End-point fluorescence was measured at 587 nm in a BioTek Synergy 4 plate reader with Gen 5 software. Glycerol measurements equalized relative to the protein content measured using a Pierce BCA Protein Assay Kit (Thermo Fisher 23225). For protein measurements, cells were lysed in mild lysis buffer (20 mM HEPES pH 7.0, 50 mM NaCl, 1 mM EDTA, 0.5 mM EGTA, 10 mM DTT, 1.0% Triton X-100, protease inhibitors), and protein measurements were taken. Colorimetric absorption was measured at 562 nm using a BioTek Synergy 4 plate reader with Gen 5 software. Statistical significance was determined using unpaired Student's *t*-test.

Larval survival assay

Second-instar larvae were collected from standard cornmeal food and transferred to lipid reduced holidic food made using the HUNTaa formulation with reduced levels (50%) of choline chloride, myo-inositol, cholesterol and sucrose (Piper et al., 2014), or holidic food supplemented with lard at 22.2 g/l (Woodcock et al., 2015). For each trial, 50 second-instar larvae from each genetic cross were transferred to holidic food or lard food. The values shown are averages from three independent genetic crosses.

Subcellular fractionation

LDs were isolated from transfected S2 cells, as described (Brasaemle and Wolins, 2016; Krahmer et al., 2011, 2013) with the following modifications. Parallel fractions were treated with 100 mN sodium carbonate, pH 11.5 (Ding et al., 2012). Cells were lysed using a 10 µm ball bearing (Isobiotec) cell homogenizer. The LD fraction was isolated, and the proteins precipitated by methanol: chloroform extraction (Wessel and Flügge, 1984). The dried protein pellet was resuspended in 30 µl gel sample buffer, boiled and size separated by SDS-PAGE. LD fractionation quality was monitored by western blotting with markers for mitochondria (CytC), ER (Cnx99A) and LDs/PLINs (Lsd-2) as well as the proportion of each protein in the LD fraction versus the pellet fraction.

Immunoblotting

Protein samples were separated by SDS-PAGE, transferred to nitrocellulose membrane (Bio-Rad 1620112), blocked in Odyssey Blocking Buffer (LI-COR) and incubated with primary antibody diluted in Blocking Buffer. Primary antibodies included guinea pig anti-Pex14 (1:2000), rabbit anti-Abcd3 primary antibody (1:1000) (Huang et al., 2020), rabbit anti Lsd-2 (1:200) (Welte et al., 2005), mouse anti-Cytochrome C (1:500, BD Pharmingen 7H8.2C12), mouse anti-Cnx99A (6-2-1, S. Munro, Developmental Studies Hybridoma Bank) and mouse anti-β-tubulin (E7, M. Klymkowsky, Developmental Studies Hybridoma Bank). For NRK cell lysates, membranes were probed with rabbit anti-PEX14 primary antibody (Thermo Fisher). Secondary antibodies used were AlexaFluor anti-rabbit A680 secondary antibody, AlexaFluor anti-mouse A790 secondary antibody, AlexaFluor anti-mouse A680 and AlexaFluor anti-guinea pig A790 (Abcam ab175773, ab186698 and Jackson ImmunoResearch 706-655-148, respectively). Membranes were visualized using an Odyssey Infrared Imaging System (LI-COR), and band intensity (relative to tubulin) was quantified using Odyssey software (LI-COR). Western blots were representative of three independent biological replicates.

Protein domain predictions

The region corresponding to the 'PEX14' domain within *Drosophila* Pex14 was predicted using Interpro annotation database (Apweiler et al., 2000), the CCD with DeepCoil2 (Ludwiczak et al., 2019) and the TM domain with TMHMM 2.0 (Krogh et al., 2001). The helical wheel projection in Fig. S7 was generated using HeliQuest (Gautier et al., 2008).

Acknowledgements

Experiments were performed with assistance from the University of Alberta Faculty of Medicine and Dentistry Cell Imaging Core, Applied Genomics Core and Flow Cytometry Facility (RRID:SCR_019195, with financial support from the Faculty of Medicine and Dentistry, University Hospital Foundation and Canada Foundation for Innovation).

Competing interests

The authors declare no competing or financial interests.

Author contributions

Conceptualization: K.U., M.N.A.-B., A.J.S.; Methodology: K.U., M.N.A.-B., A.J.S.; Validation: A.J.S.; Formal analysis: K.U., M.N.A.-B., A.J.S.; Investigation: K.U., M.N.A.-B., J.H., A.J.S.; Resources: J.H., S.C.H., A.J.S.; Writing - original draft: K.U., M.N.A.-B., A.J.S.; Writing - review & editing: K.U., M.N.A.-B., S.C.H., A.J.S.; Visualization: M.N.A.-B., A.J.S.; Supervision: A.J.S.; Project administration: A.J.S.; Funding acquisition: S.C.H., A.J.S.

Funding

This work was supported by Discovery Grants from the Natural Sciences and Engineering Research Council of Canada to A.J.S. (RGPIN-2017-05885) and S.C.H. (RGPIN-2021-02873), a Canadian Graduate studentship from the Canadian Institutes of Health Research to K.U. and M.N.A.-B., and a Women and Children's Health Research Institute Graduate Studentship funded through the Stollery Children's Hospital Foundation to K.U.

Data availability

RNASeq data are available in the NCBI BioProject database (PRJNA807290).

Peer review history

The peer review history is available online at https://journals.biologists.com/jcs/article-lookup/doi/10.1242/jcs.259092.

References

Adler, J. and Parmryd, I. (2010). Quantifying colocalization by correlation: the Pearson correlation coefficient is superior to the Mander's overlap coefficient. *Cytometry A* **77**, 733-742. doi:10.1002/cyto.a.20896

Anders, S., Pyl, P. T. and Huber, W. (2015). HTSeq–a Python framework to work with high-throughput sequencing data. *Bioinformatics* **31**, 166-169. doi:10.1093/bioinformatics/btu638

Anderson-Baron, M. N. and Simmonds, A. J. (2019). Peroxisome protein prediction in Drosophila melanogaster. In *Proteomics of Peroxisomes: Identifying Novel Functions and Regulatory Networks*, Vol. 89 (ed. L. A. del Rio and M. Schrader), pp. 1-25. Singapore: Springer Nature Singapore Pte Ltd.

Apweiler, R., Attwood, T. K., Bairoch, A., Bateman, A., Birney, E., Biswas, M., Bucher, P., Cerutti, L., Corpet, F., Croning, M. D. R. et al. (2000). InterPro–an integrated documentation resource for protein families, domains and functional sites. *Bioinformatics* **16**, 1145-1150. doi:10.1093/bioinformatics/16.12.1145

Aranovich, A., Hua, R., Rutenberg, A. D. and Kim, P. K. (2014). PEX16 contributes to peroxisome maintenance by constantly trafficking PEX3 via the ER. *J. Cell Sci.* **127**, 3675-3686. doi:10.1242/jcs.146282

Azevedo, J. E. and Schliebs, W. (2006). Pex14p, more than just a docking protein. *Biochim. Biophys. Acta* **1763**, 1574-1584. doi:10.1016/j.bbamcr.2006.09.002

Baron, M. N., Klinger, C. M., Rachubinski, R. A. and Simmonds, A. J. (2016). A systematic cell-based analysis of localization of predicted Drosophila Peroxisomal proteins. *Traffic* **17**, 536-553. doi:10.1111/tra.12384

Barros-Barbosa, A., Rodrigues, T. A., Ferreira, M. J., Pedrosa, A. G., Teixeira, N. R., Francisco, T. and Azevedo, J. E. (2019). The intrinsically disordered nature of the peroxisomal protein translocation machinery. *FEBS J.* **286**, 24-38. doi:10.1111/febs.14704

Beller, M., Riedel, D., Jänsch, L., Dieterich, G., Wehland, J., Jäckle, H. and Kühnlein, R. P. (2006). Characterization of the Drosophila lipid droplet subproteome. *Mol. Cell. Proteomics* **5**, 1082-1094. doi:10.1074/mcp.M600011-MCP200

Beller, M., Bulankina, A. V., Hsiao, H.-H., Urlaub, H., Jäckle, H. and Kühnlein, R. P. (2010). PERILIPIN-dependent control of lipid droplet structure and fat storage in Drosophila. *Cell Metab.* **12**, 521-532. doi:10.1016/j.cmet.2010.10.001

Bharti, P., Schliebs, W., Schievelbusch, T., Neuhaus, A., David, C., Kock, K., Herrmann, C., Meyer, H. E., Wiese, S., Warscheid, B. et al. (2011). PEX14 is required for microtubule-based peroxisome motility in human cells. *J. Cell Sci.* **124**, 1759-1768. doi:10.1242/jcs.079368

Bi, J., Xiang, Y., Chen, H., Liu, Z., Grönke, S., Kühnlein, R. P. and Huang, X. (2012). Opposite and redundant roles of the two Drosophila perilipins in lipid mobilization. *J. Cell Sci.* **125**, 3568-3577. doi:10.1242/jcs.101329

Binns, D., Januszewski, T., Chen, Y., Hill, J., Markin, V. S., Zhao, Y., Gilpin, C., Chapman, K. D., Anderson, R. G. W. and Goodman, J. M. (2006). An intimate

collaboration between peroxisomes and lipid bodies. *J. Cell Biol.* **173**, 719-731. doi:10.1083/jcb.200511125

Brasaemle, D. L. and Wolins, N. E. (2016). Isolation of lipid droplets from cells by density gradient centrifugation. *Curr. Protoc. Cell Biol.* **72**, 3.15.1-3.15.13. doi:10.1002/cpcb.10

Bülow, M. H., Wingen, C., Senyilmaz, D., Gosejacob, D., Sociale, M., Bauer, R., Schulze, H., Sandhoff, K., Teleman, A. A., Hoch, M. et al. (2018). Unbalanced lipolysis results in lipotoxicity and mitochondrial damage in peroxisome-deficient Pex19 mutants. *Mol. Biol. Cell* **29**, 396-407. doi:10.1091/mbc.E17-08-0535

Cermelli, S., Guo, Y., Gross, S. P. and Welte, M. A. (2006). The lipid-droplet proteome reveals that droplets are a protein-storage depot. *Curr. Biol.* **16**, 1783-1795. doi:10.1016/j.cub.2006.07.062

Chang, C.-L., Weigel, A. V., Ioannou, M. S., Pasolli, H. A., Xu, C. S., Peale, D. R., Shtengel, G., Freeman, M., Hess, H. F., Blackstone, C. et al. (2019). Spastin tethers lipid droplets to peroxisomes and directs fatty acid trafficking through ESCRT-III. *J. Cell Biol.* **218**, jcb.201902061. doi:10.1083/jcb.201902061

Chen, H., Liu, Z. and Huang, X. (2010). Drosophila models of peroxisomal biogenesis disorder: peroxins are required for spermatogenesis and very-long-chain fatty acid metabolism. *Hum. Mol. Genet.* **19**, 494-505. doi:10.1093/hmg/ddp518

Cheng, X., Yan, J., Liu, Y., Wang, J. and Taubert, S. (2021). eVITTA: a web-based visualization and inference toolbox for transcriptome analysis. *Nucleic Acids Res.* **49**, W207-W215. doi:10.1093/nar/gkab366

Choudhary, V. and Schneiter, R. (2021). A unique junctional interface at contact sites between the endoplasmic reticulum and lipid droplets. *Front. Cell Dev. Biol.* **9**, 650186. doi:10.3389/fcell.2021.650186

Church, R. B. and Robertson, F. W. (1966). Biochemical analysis of genetic differences in the growth of Drosophila. *Genet. Res.* **7**, 383-407. doi:10.1017/S0016672300009836

Dahan, N., Bykov, Y. S., Boydston, E. A., Fadel, A., Gazi, Z., Hochberg-Laufer, H., Martenson, J., Denic, V., Shav-Tal, Y., Weissman, J. S. et al. (2022). Peroxisome function relies on organelle-associated mRNA translation. *Sci. Adv.* **8**, eabk2141. doi:10.1126/sciadv.abk2141

Darfler, P. J. (1990). Preparation and use of lipid microemulsions as nutritional supplements for culturing mammalian cells. *In Vitro Cell Dev. Biol.* **26**, 779-783. doi:10.1007/BF02623619

Di Cara, F., Sheshachalam, A., Braverman, N. E., Rachubinski, R. A. and Simmonds, A. J. (2017). Peroxisome-Mediated Metabolism Is Required for Immune Response to Microbial Infection. *Immunity* **47**, 93-106.e7. doi:10.1016/j.immuni.2017.06.016

Di Cara, F., Rachubinski, R. A. and Simmonds, A. J. (2019). Distinct roles for peroxisomal targeting signal receptors Pex5 and Pex7 in Drosophila. *Genetics* **211**, 141-149. doi:10.1534/genetics.118.301628

Ding, Y., Wu, Y., Zeng, R. and Liao, K. (2012). Proteomic profiling of lipid droplet-associated proteins in primary adipocytes of normal and obese mouse. *Acta Biochim. Biophys. Sin.* **44**, 394-406. doi:10.1093/abbs/gms008

Ding, L., Sun, W., Balaz, M., He, A., Klug, M., Wieland, S., Caiazzo, R., Raverdy, V., Pattou, F., Lefebvre, P. et al. (2021). Peroxisomal β-oxidation acts as a sensor for intracellular fatty acids and regulates lipolysis. *Nat. Metab.* **3**, 1648-1661. doi:10.1038/s42255-021-00489-2

Ducharme, N. A. and Bickel, P. E. (2008). Lipid droplets in lipogenesis and lipolysis. *Endocrinology* **149**, 942-949. doi:10.1210/en.2007-1713

Dunn, K. W., Kamocka, M. M. and McDonald, J. H. (2011). A practical guide to evaluating colocalization in biological microscopy. *Am. J. Physiol. Cell Physiol.* **300**, C723-C742. doi:10.1152/ajpcell.00462.2010

Fakieh, M. H., Drake, P. J. M., Lacey, J., Munck, J. M., Motley, A. M. and Hettema, E. H. (2013). Intra-ER sorting of the peroxisomal membrane protein Pex3 relies on its luminal domain. *Biol. Open* **2**, 829-837. doi:10.1242/bio.20134788

Fang, Y., Morrell, J. C., Jones, J. M. and Gould, S. J. (2004). PEX3 functions as a PEX19 docking factor in the import of class I peroxisomal membrane proteins. *J. Cell Biol.* **164**, 863-875. doi:10.1083/jcb.200311131

Faust, J. E., Verma, A., Peng, C. and McNew, J. A. (2012). An inventory of peroxisomal proteins and pathways in Drosophila melanogaster. *Traffic* **13**, 1378-1392. doi:10.1111/j.1600-0854.2012.01393.x

Faust, J. E., Manisundaram, A., Ivanova, P. T., Milne, S. B., Summerville, J. B., Brown, H. A., Wangler, M., Stern, M. and McNew, J. A. (2014). Peroxisomes are required for lipid metabolism and muscle function in Drosophila melanogaster. *PLoS ONE* **9**, e100213. doi:10.1371/journal.pone.0100213

Foley, E. and O'Farrell, P. H. (2004). Functional dissection of an innate immune response by a genome-wide RNAi screen. *PLoS Biol.* **2**, E203. doi:10.1371/journal.pbio.0020203

Fujiki, Y., Abe, Y., Imoto, Y., Tanaka, A. J., Okumoto, K., Honsho, M., Tamura, S., Miyata, N., Yamashita, T., Chung, W. K. et al. (2020). Recent insights into peroxisome biogenesis and associated diseases. *J. Cell Sci.* **133**, jcs236943. doi:10.1242/jcs.236943

Fujimoto, T. and Parton, R. G. (2011). Not just fat: the structure and function of the lipid droplet. *Cold Spring Harb. Perspect. Biol.* **3**, a004838. doi:10.1101/cshperspect.a004838

Gaussmann, S., Gopalswamy, M., Eberhardt, M., Reuter, M., Zou, P., Schliebs, W., Erdmann, R. and Sattler, M. (2021). Membrane interactions of the peroxisomal proteins PEX5 and PEX14. *Front. Cell Dev. Biol.* **9**, 651449. doi:10.3389/fcell.2021.651449

Gautier, R., Douguet, D., Antonny, B. and Drin, G. (2008). HELIQUEST: a web server to screen sequences with specific alpha-helical properties. *Bioinformatics* **24**, 2101-2102. doi:10.1093/bioinformatics/btn392

Geuze, H. J., Murk, J. L., Stroobants, A. K., Griffith, J. M., Kleijmeer, M. J., Koster, A. J., Verkleij, A. J., Distel, B. and Tabak, H. F. (2003). Involvement of the endoplasmic reticulum in peroxisome formation. *Mol. Biol. Cell* **14**, 2900-2907. doi:10.1091/mbc.e02-11-0734

Goedhart, J. (2021). SuperPlotsOfData-a web app for the transparent display and quantitative comparison of continuous data from different conditions. *Mol. Biol. Cell* **32**, 470-474. doi:10.1091/mbc.E20-09-0583

Grönke, S., Mildner, A., Fellert, S., Tennagels, N., Petry, S., Müller, G., Jackle, H. and Kühnlein, R. P. (2005). Brummer lipase is an evolutionary conserved fat storage regulator in Drosophila. *Cell Metab.* **1**, 323-330. doi:10.1016/j.cmet.2005.04.003

Guo, Y., Walther, T. C., Rao, M., Stuurman, N., Goshima, G., Terayama, K., Wong, J. S., Vale, R. D., Walter, P. and Farese, R. V. (2008). Functional genomic screen reveals genes involved in lipid-droplet formation and utilization. *Nature* **453**, 657-661. doi:10.1038/nature06928

He, A., Dean, J. M. and Lodhi, I. J. (2021). Peroxisomes as cellular adaptors to metabolic and environmental stress. *Trends Cell Biol.* **31**, 656-670. doi:10.1016/j.tcb.2021.02.005

Heier, C. and Kühnlein, R. P. (2018). Triacylglycerol metabolism in *Drosophila melanogaster*. *Genetics* **210**, 1163. doi:10.1534/genetics.118.301583

Honsho, M., Yamashita, S.-I. and Fujiki, Y. (2016). Peroxisome homeostasis: mechanisms of division and selective degradation of peroxisomes in mammals. *Biochim. Biophys. Acta* **1863**, 984-991. doi:10.1016/j.bbamcr.2015.09.032

Hu, Y., Sopko, R., Foos, M., Kelley, C., Flockhart, I., Ammeux, N., Wang, X., Perkins, L., Perrimon, N. and Mohr, S. E. (2013). FlyPrimerBank: an online database for Drosophila melanogaster gene expression analysis and knockdown evaluation of RNAi reagents. *G3 (Bethesda)* **3**, 1607-1616. doi:10.1534/g3.113.007021

Huang, K., Miao, T., Chang, K., Kim, J., Kang, P., Jiang, Q., Simmonds, A. J., Di Cara, F. and Bai, H. (2020). Impaired peroxisomal import in Drosophila oenocytes causes cardiac dysfunction by inducing upd3 as a peroxikine. *Nat. Commun.* **11**, 2943. doi:10.1038/s41467-020-16781-w

Itabe, H., Yamaguchi, T., Nimura, S. and Sasabe, N. (2017). Perilipins: a diversity of intracellular lipid droplet proteins. *Lipids Health Dis.* **16**, 83. doi:10.1186/s12944-017-0473-y

Itoh, R. and Fujiki, Y. (2006). Functional domains and dynamic assembly of the peroxin Pex14p, the entry site of matrix proteins. *J. Biol. Chem.* **281**, 10196-10205. doi:10.1074/jbc.M600158200

Jackson, C. L. (2019). Lipid droplet biogenesis. *Curr. Opin. Cell Biol.* **59**, 88-96. doi:10.1016/j.ceb.2019.03.018

Joshi, A. S. and Cohen, S. (2019). Lipid droplet and peroxisome biogenesis: do they go hand-in-hand? *Front. Cell Dev. Biol.* **7**, 92. doi:10.3389/fcell.2019.00092

Kim, P. (2017). Peroxisome biogenesis: a union between two organelles. *Curr. Biol.* **27**, R271-R274. doi:10.1016/j.cub.2017.02.052

Kim, D., Langmead, B. and Salzberg, S. L. (2015). HISAT: a fast spliced aligner with low memory requirements. *Nat. Methods* **12**, 357-360. doi:10.1038/nmeth.3317

Kong, J., Ji, Y., Jeon, Y. G., Han, J. S., Han, K. H., Lee, J. H., Lee, G., Jang, H., Choe, S. S., Baes, M. et al. (2020). Spatiotemporal contact between peroxisomes and lipid droplets regulates fasting-induced lipolysis via PEX5. *Nat. Commun.* **11**, 578. doi:10.1038/s41467-019-14176-0

Kory, N., Thiam, A.-R., Farese, R. V., Jr and Walther, T. C. (2015). Protein crowding is a determinant of lipid droplet protein composition. *Dev. Cell* **34**, 351-363. doi:10.1016/j.devcel.2015.06.007

Krahmer, N., Guo, Y., Wilfling, F., Hilger, M., Lingrell, S., Heger, K., Newman, H. W., Schmidt-Supprian, M., Vance, D. E., Mann, M. et al. (2011). Phosphatidylcholine synthesis for lipid droplet expansion is mediated by localized activation of CTP:phosphocholine cytidylyltransferase. *Cell Metab.* **14**, 504-515. doi:10.1016/j.cmet.2011.07.013

Krahmer, N., Hilger, M., Kory, N., Wilfling, F., Stoehr, G., Mann, M., Farese, R. V., Jr and Walther, T. C. (2013). Protein correlation profiles identify lipid droplet proteins with high confidence. *Mol. Cell. Proteomics* **12**, 1115-1126. doi:10.1074/mcp.M112.020230

Kramer, D. A., Quiroga, A. D., Lian, J., Fahlman, R. P. and Lehner, R. (2018). Fasting and refeeding induces changes in the mouse hepatic lipid droplet proteome. *J. Proteomics* **181**, 213-224. doi:10.1016/j.jprot.2018.04.024

Krogh, A., Larsson, B., von Heijne, G. and Sonnhammer, E. L. L. (2001). Predicting transmembrane protein topology with a hidden Markov model: application to complete genomes. *J. Mol. Biol.* **305**, 567-580. doi:10.1006/jmbi.2000.4315

Kuhnlein, R. P. (2012). Thematic review series: lipid droplet synthesis and metabolism: from yeast to man. Lipid droplet-based storage fat metabolism in Drosophila. *J. Lipid Res.* **53**, 1430-1436. doi:10.1194/jlr.R024299

Kunze, M. (2020). The type-2 peroxisomal targeting signal. *Biochim. Biophys. Acta Mol. Cell Res.* **1867**, 118609. doi:10.1016/j.bbamcr.2019.118609
Lass, A., Zimmermann, R., Oberer, M. and Zechner, R. (2011). Lipolysis - a highly regulated multi-enzyme complex mediates the catabolism of cellular fat stores. *Prog. Lipid Res.* **50**, 14-27. doi:10.1016/j.plipres.2010.10.004
Leznicki, P., Schneider, H. O., Harvey, J. V., Shi, W. Q. and High, S. (2022). Co-translational biogenesis of lipid droplet integral membrane proteins. *J. Cell Sci.* **135**, jcs259220. doi:10.1242/jcs.259220
Liu, Y., Weaver, C. M., Sen, Y., Eitzen, G., Simmonds, A. J., Linchieh, L., Lurette, O., Hebert-Chatelain, E., Rachubinski, R. A. and Di Cara, F. (2021). The nitric oxide donor, S-Nitrosoglutathione, rescues peroxisome number and activity defects in PEX1G843D mild Zellweger Syndrome fibroblasts. *Front. Cell Dev. Biol.* **9**, 714710. doi:10.3389/fcell.2021.714710
Lodhi, I. J. and Semenkovich, C. F. (2014). Peroxisomes: a nexus for lipid metabolism and cellular signaling. *Cell Metab.* **19**, 380-392. doi:10.1016/j.cmet.2014.01.002
Love, M. I., Huber, W. and Anders, S. (2014). Moderated estimation of fold change and dispersion for RNA-seq data with DESeq2. *Genome Biol.* **15**, 550. doi:10.1186/s13059-014-0550-8
Ludwiczak, J., Winski, A., Szczepaniak, K., Alva, V. and Dunin-Horkawicz, S. (2019). DeepCoil-a fast and accurate prediction of coiled-coil domains in protein sequences. *Bioinformatics* **35**, 2790-2795. doi:10.1093/bioinformatics/bty1062
Luhur, A., Klueg, K. M. and Zelhof, A. C. (2019). Generating and working with *Drosophila* cell cultures: Current challenges and opportunities. *Wiley Interdiscip. Rev. Dev. Biol.* **8**, e339. doi:10.1002/wdev.339
Marcinkiewicz, A., Gauthier, D., Garcia, A. and Brasaemle, D. L. (2006). The phosphorylation of serine 492 of perilipin a directs lipid droplet fragmentation and dispersion. *J. Biol. Chem.* **281**, 11901-11909. doi:10.1074/jbc.M600171200
Mast, F. D., Li, J., Virk, M. K., Hughes, S. C., Simmonds, A. J. and Rachubinski, R. A. (2011). A *Drosophila* model for the Zellweger spectrum of peroxisome biogenesis disorders. *Dis. Model. Mech.* **4**, 659-672. doi:10.1242/dmm.007419
Matsuzaki, T. and Fujiki, Y. (2008). The peroxisomal membrane protein import receptor Pex3p is directly transported to peroxisomes by a novel Pex19p- and Pex16p-dependent pathway. *J. Cell Biol.* **183**, 1275-1286. doi:10.1083/jcb.200806062
Musselman, L. P. and Kuhnlein, R. P. (2018). *Drosophila* as a model to study obesity and metabolic disease. *J. Exp. Biol.* **221**, jeb163881. doi:10.1242/jeb.163881
Nakayama, M., Sato, H., Okuda, T., Fujisawa, N., Kono, N., Arai, H., Suzuki, E., Umeda, M., Ishikawa, H. O. and Matsuno, K. (2011). *Drosophila* carrying pex3 or pex16 mutations are models of Zellweger syndrome that reflect its symptoms associated with the absence of peroxisomes. *PLoS ONE* **6**, e22984. doi:10.1371/journal.pone.0022984
Natsuyama, R., Okumoto, K. and Fujiki, Y. (2013). Pex5p stabilizes Pex14p: a study using a newly isolated pex5 CHO cell mutant, ZPEG101. *Biochem. J.* **449**, 195-207. doi:10.1042/BJ20120911
Neufeld, C., Filipp, F. V., Simon, B., Neuhaus, A., Schüller, N., David, C., Kooshapur, H., Madl, T., Erdmann, R., Schliebs, W. et al. (2009). Structural basis for competitive interactions of Pex14 with the import receptors Pex5 and Pex19. *EMBO J.* **28**, 745-754. doi:10.1038/emboj.2009.7
Nordgren, M., Wang, B., Apanasets, O. and Fransen, M. (2013). Peroxisome degradation in mammals: mechanisms of action, recent advances, and perspectives. *Front. Physiol.* **4**, 145. doi:10.3389/fphys.2013.00145
Olzmann, J. A. and Carvalho, P. (2019). Dynamics and functions of lipid droplets. *Nat. Rev. Mol. Cell Biol.* **20**, 137-155. doi:10.1038/s41580-018-0085-z
Otera, H., Setoguchi, K., Hamasaki, M., Kumashiro, T., Shimizu, N. and Fujiki, Y. (2002). Peroxisomal targeting signal receptor Pex5p interacts with cargoes and import machinery components in a spatiotemporally differentiated manner: conserved Pex5p WXXXF/Y motifs are critical for matrix protein import. *Mol. Cell. Biol.* **22**, 1639-1655. doi:10.1128/MCB.22.6.1639-1655.2002
Piper, M. D. W., Blanc, E., Leitão-Gonçalves, R., Yang, M., He, X., Linford, N. J., Hoddinott, M. P., Hopfen, C., Soultoukis, G. A., Niemeyer, C. et al. (2014). A holidic medium for *Drosophila melanogaster*. *Nat. Methods* **11**, 100-105. doi:10.1038/nmeth.2731
Pridie, C., Ueda, K. and Simmonds, A. J. (2020). Rosy beginnings: studying peroxisomes in *Drosophila*. *Front. Cell Dev. Biol.* **8**, 835. doi:10.3389/fcell.2020.00835
Reis, T., Van Gilst, M. R. and Hariharan, I. K. (2010). A buoyancy-based screen of *Drosophila* larvae for fat-storage mutants reveals a role for Sir2 in coupling fat storage to nutrient availability. *PLoS Genet.* **6**, e1001206. doi:10.1371/journal.pgen.1001206
Reuter, M., Kooshapur, H., Suda, J.-G., Gaussmann, S., Neuhaus, A., Brühl, L., Bharti, P., Jung, M., Schliebs, W., Sattler, M. et al. (2021). Competitive microtubule binding of PEX14 coordinates peroxisomal protein import and motility. *J. Mol. Biol.* **433**, 166765. doi:10.1016/j.jmb.2020.166765
Robinson, M. D., McCarthy, D. J. and Smyth, G. K. (2010). EdgeR: a Bioconductor package for differential expression analysis of digital gene expression data. *Bioinformatics* **26**, 139-140. doi:10.1093/bioinformatics/btp616
Rogers, S. L., Rogers, G. C., Sharp, D. J. and Vale, R. D. (2002). *Drosophila* EB1 is important for proper assembly, dynamics, and positioning of the mitotic spindle. *J. Cell Biol.* **158**, 873-884. doi:10.1083/jcb.200202032
Rucktaschel, R., Halbach, A., Girzalsky, W., Rottensteiner, H. and Erdmann, R. (2010). De novo synthesis of peroxisomes upon mitochondrial targeting of Pex3p. *Eur. J. Cell Biol.* **89**, 947-954. doi:10.1016/j.ejcb.2010.06.012
Sacksteder, K. A., Jones, J. M., South, S. T., Li, X., Liu, Y. and Gould, S. J. (2000). PEX19 binds multiple peroxisomal membrane proteins, is predominantly cytoplasmic, and is required for peroxisome membrane synthesis. *J. Cell Biol.* **148**, 931-944. doi:10.1083/jcb.148.5.931
Samis, H. V., Baird, M. B. and Massie, H. R. (1972). Renewal of catalase activity in *Drosophila* following treatment with 3-amino-1,2,4-triazole. *J. Insect Physiol.* **18**, 991-1000. doi:10.1016/0022-1910(72)90036-4
Schneider, I. (1972). Cell lines derived from late embryonic stages of *Drosophila melanogaster*. *J. Embryol. Exp. Morphol.* **27**, 353-365. doi:10.1242/dev.27.2.353
Schrader, M. (2001). Tubulo-reticular clusters of peroxisomes in living COS-7 cells: dynamic behavior and association with lipid droplets. *J. Histochem. Cytochem.* **49**, 1421-1429. doi:10.1177/002215540104901110
Schrader, M., Costello, J. L., Godinho, L. F., Azadi, A. S. and Islinger, M. (2016). Proliferation and fission of peroxisomes - an update. *Biochim. Biophys. Acta* **1863**, 971-983. doi:10.1016/j.bbamcr.2015.09.024
Schrul, B. and Kopito, R. R. (2016). Peroxin-dependent targeting of a lipid-droplet-destined membrane protein to ER subdomains. *Nat. Cell Biol.* **18**, 740-751. doi:10.1038/ncb3373
Sellin, J., Wingen, C., Gosejacob, D., Senyilmaz, D., Hänschke, L., Büttner, S., Meyer, K., Bano, D., Nicotera, P., Teleman, A. A. et al. (2018). Dietary rescue of lipotoxicity-induced mitochondrial damage in Peroxin19 mutants. *PLoS Biol.* **16**, e2004893. doi:10.1371/journal.pbio.2004893
Sugiura, A., Mattie, S., Prudent, J. and McBride, H. M. (2017). Newly born peroxisomes are a hybrid of mitochondrial and ER-derived pre-peroxisomes. *Nature* **542**, 251-254. doi:10.1038/nature21375
Sui, X., Arlt, H., Brock, K. P., Lai, Z. W., DiMaio, F., Marks, D. S., Liao, M., Farese, R. V., Jr and Walther, T. C. (2018). Cryo-electron microscopy structure of the lipid droplet-formation protein seipin. *J. Cell Biol.* **217**, 4080-4091. doi:10.1083/jcb.201809067
Tennessen, J. M., Barry, W. E., Cox, J. and Thummel, C. S. (2014). Methods for studying metabolism in *Drosophila*. *Methods* **68**, 105-115. doi:10.1016/j.ymeth.2014.02.034
Thiam, A. R. and Dugail, I. (2019). Lipid droplet-membrane contact sites - from protein binding to function. *J. Cell Sci.* **132**, jcs230169. doi:10.1242/jcs.230169
van der Zand, A. and Tabak, H. F. (2013). Peroxisomes: offshoots of the ER. *Curr. Opin. Cell Biol.* **25**, 449-454. doi:10.1016/j.ceb.2013.05.004
van der Zand, A., Braakman, I. and Tabak, H. F. (2010). Peroxisomal membrane proteins insert into the endoplasmic reticulum. *Mol. Biol. Cell* **21**, 2057-2065. doi:10.1091/mbc.e10-02-0082
Varet, H., Brillet-Guéguen, L., Coppée, J.-Y. and Dillies, M.-A. (2016). SARTools: a DESeq2- and EdgeR-Based R pipeline for comprehensive differential analysis of RNA-Seq data. *PLoS ONE* **11**, e0157022. doi:10.1371/journal.pone.0157022
Walther, T. C., Chung, J. and Farese, R. V.Jr. (2017). Lipid droplet biogenesis. *Annu. Rev. Cell Dev. Biol.* **33**, 491-510. doi:10.1146/annurev-cellbio-100616-060608
Wang, H., Becuwe, M., Housden, B. E., Chitraju, C., Porras, A. J., Graham, M. M., Liu, X. N., Thiam, A. R., Savage, D. B., Agarwal, A. K. et al. (2016). Seipin is required for converting nascent to mature lipid droplets. *eLife* **5**, e16582. doi:10.7554/eLife.16582
Welte, M. A., Cermelli, S., Griner, J., Viera, A., Guo, Y., Kim, D.-H., Gindhart, J. G. and Gross, S. P. (2005). Regulation of lipid-droplet transport by the perilipin homolog LSD2. *Curr. Biol.* **15**, 1266-1275. doi:10.1016/j.cub.2005.06.062
Wessel, D. and Flügge, U. I. (1984). A method for the quantitative recovery of protein in dilute solution in the presence of detergents and lipids. *Anal. Biochem.* **138**, 141-143. doi:10.1016/0003-2697(84)90782-6
Wilfling, F., Wang, H., Haas, J. T., Krahmer, N., Gould, T. J., Uchida, A., Cheng, J.-X., Graham, M., Christiano, R., Frohlich, F. et al. (2013). Triacylglycerol synthesis enzymes mediate lipid droplet growth by relocalizing from the ER to lipid droplets. *Dev. Cell* **24**, 384-399. doi:10.1016/j.devcel.2013.01.013
Wilfling, F., Haas, J. T., Walther, T. C. and Farese, R. V.Jr. (2014). Lipid droplet biogenesis. *Curr. Opin. Cell Biol.* **29**, 39-45. doi:10.1016/j.ceb.2014.03.008
Will, G. K., Soukupova, M., Hong, X., Erdmann, K. S., Kiel, J. A. K. W., Dodt, G., Kunau, W.-H. and Erdmann, R. (1999). Identification and characterization of the human orthologue of yeast Pex14p. *Mol. Cell. Biol.* **19**, 2265-2277. doi:10.1128/MCB.19.3.2265
Woodcock, K. J., Kierdorf, K., Pouchelon, C. A., Vivancos, V., Dionne, M. S. and Geissmann, F. (2015). Macrophage-derived upd3 cytokine causes impaired glucose homeostasis and reduced lifespan in *Drosophila* fed a lipid-rich diet. *Immunity* **42**, 133-144. doi:10.1016/j.immuni.2014.12.023
Zimmermann, R., Strauss, J. G., Haemmerle, G., Schoiswohl, G., Birner-Gruenberger, R., Riederer, M., Lass, A., Neuberger, G., Eisenhaber, F., Hermetter, A. et al. (2004). Fat mobilization in adipose tissue is promoted by adipose triglyceride lipase. *Science* **306**, 1383. doi:10.1126/science.1100747

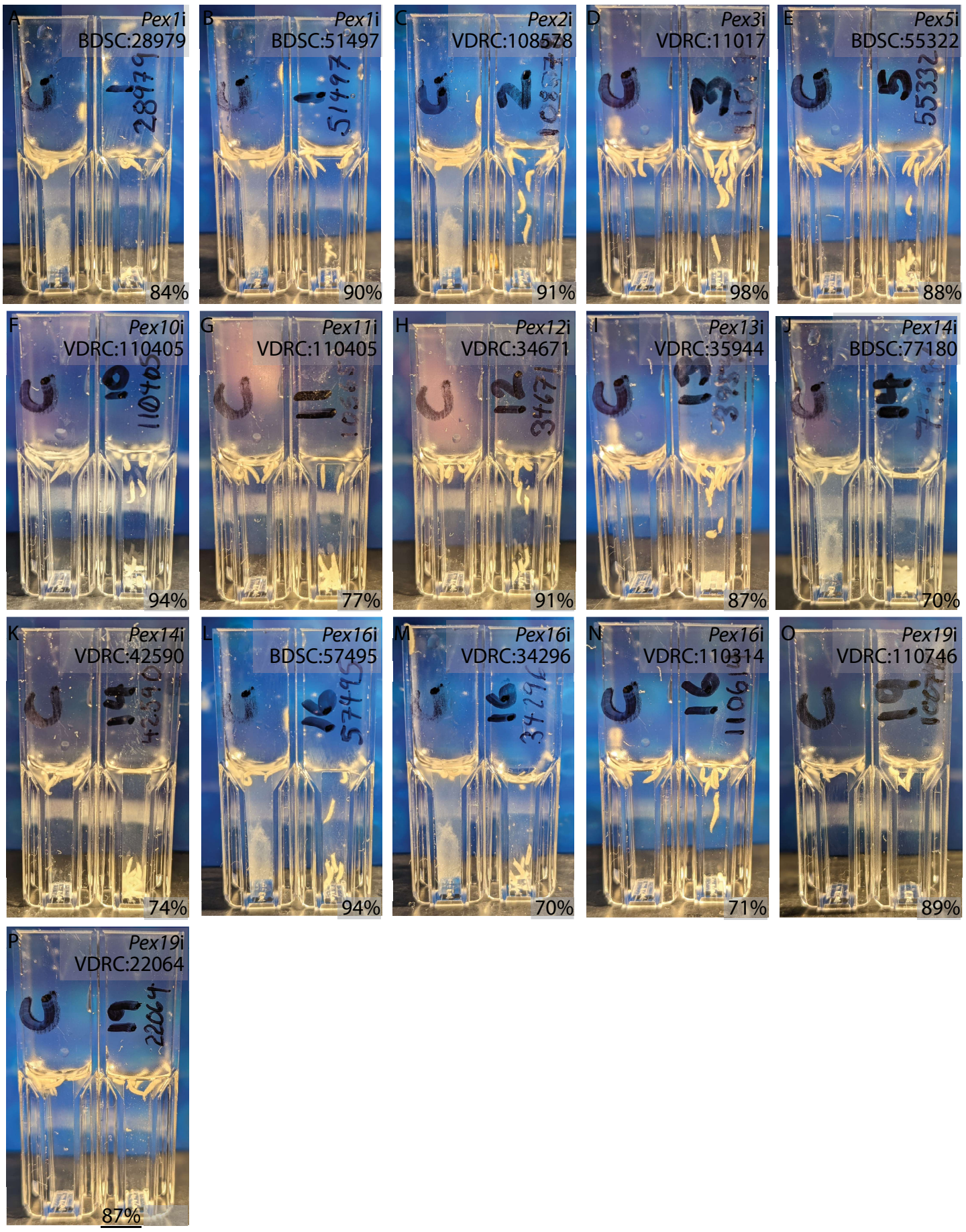
A
Pex1i
BDSC:28979
84%
B
Pex1i
BDSC:51497
90%
C
Pex2i
VDRC:108578
91%
D
Pex3i
VDRC:11017
98%
E
Pex5i
BDSC:55322
88%
F
Pex10i
VDRC:110405
94%
G
Pex11i
VDRC:110405
77%
H
Pex12i
VDRC:34671
91%
I
Pex13i
VDRC:35944
87%
J
Pex14i
BDSC:77180
70%
K
Pex14i
VDRC:42590
74%
L
Pex16i
BDSC:57495
94%
M
Pex16i
VDRC:34296
70%
N
Pex16i
VDRC:110314
71%
O
Pex19i
VDRC:110746
89%
P
Pex19i
VDRC:22064
87%

Fig. S1. Representative images from a small-scale screen for the effect of fat body targeted Peroxin lipid storage. The r4-GAL4 driver line and UAS-transgenes expressing double stranded RNA targeting each *Pex* gene were used (See Figure 1 B-C). The value at the bottom of each image indicates the efficiency of knockdown confirmed by qRTPCR in larvae where the UAS-RNAi transgene was expressed ubiquitously via Tub-GAL4. Larvae with normal fat storage float in 12% sucrose. For each image, the cuvette shown on the right is the *Pex*i larvae and, on the left, (labelled C) control r4-GAL4 larvae suspended in a 12% sucrose solution. The unique VDRC or BDRC stock centre ID for each RNAi transgene is provided. The number in brackets under the *Pex* gene number on each cuvette indicates a serial number used for experimental blinding. The position of the larvae in each cuvette was recorded in terms of quartiles representing distance from the surface of the sucrose solution to the bottom.

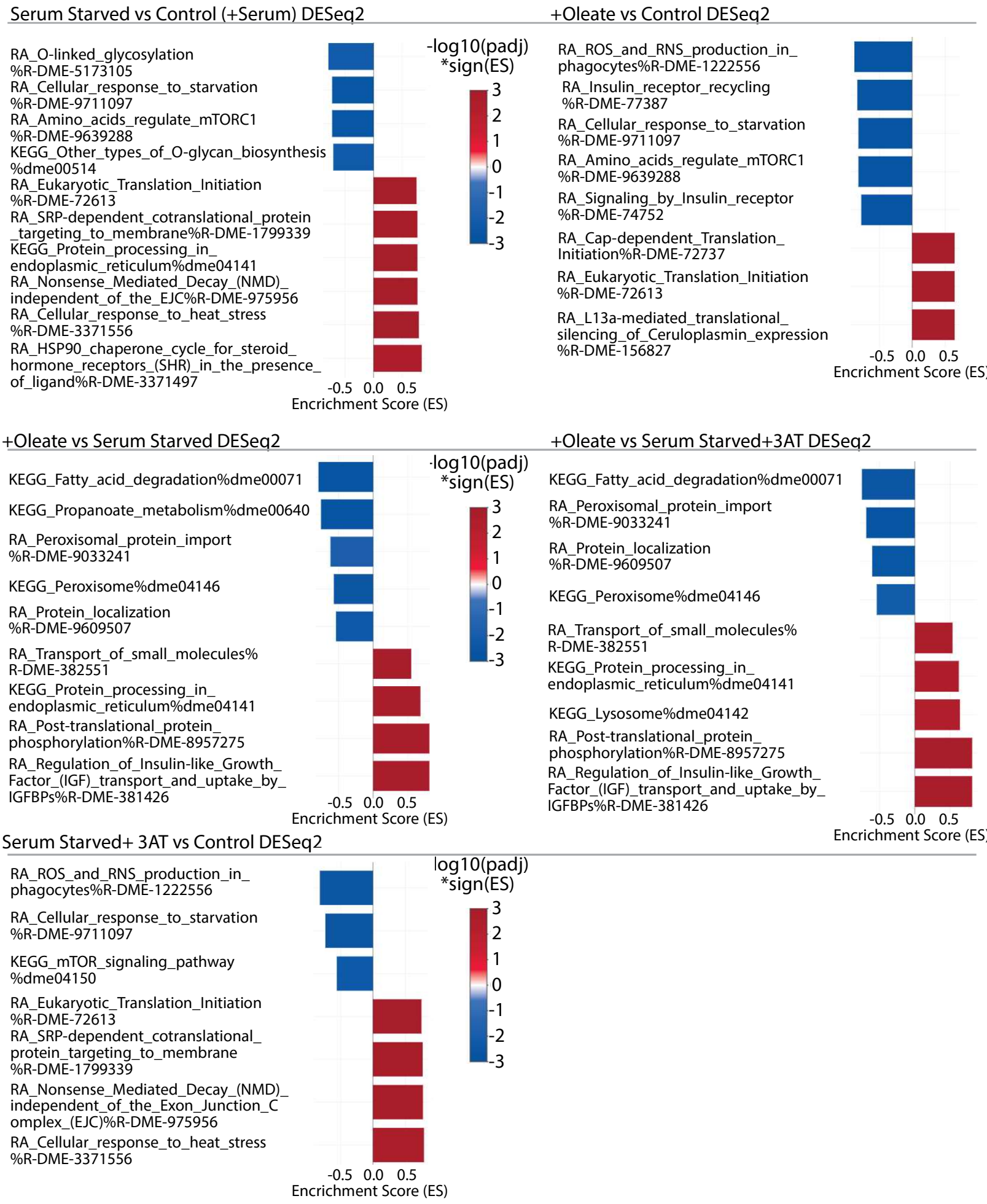
Serum Starved vs Control (+Serum) DESeq2
RA_O-linked_glycosylation %R-DME-5173105
RA_Cellular_response_to_starvation %R-DME-9711097
RA_Amino_acids_regulate_mTORC1 %R-DME-9639288
KEGG_Other_types_of_O-glycan_biosynthesis %dme00514
RA_Eukaryotic_Translation_Initiation %R-DME-72613
RA_SRP-dependent_cotranslational_protein _targeting_to_membrane%R-DME-1799339
KEGG_Protein_processing_in_ endoplasmic_reticulum%dme04141
RA_Nonsense_Mediated_Decay_(NMD)_ independent_of_the_EJC%R-DME-975956
RA_Cellular_response_to_heat_stress %R-DME-3371556
RA_HSP90_chaperone_cycle_for_steroid_ hormone_receptors_(SHR)_in_the_presence_ of_ligand%R-DME-3371497
-log10(padj) *sign(ES)
3
2
1
0
-1
-2
-3
-0.5 0.0 0.5
Encrichment Score (ES)
+Oleate vs Control DESeq2
RA_ROS_and_RNS_production_in_ phagocytes%R-DME-1222556
RA_Insulin_receptor_recycling %R-DME-77387
RA_Cellular_response_to_starvation %R-DME-9711097
RA_Amino_acids_regulate_mTORC1 %R-DME-9639288
RA_Signaling_by_Insulin_receptor %R-DME-74752
RA_Cap-dependent_Translation_ Initiation%R-DME-72737
RA_Eukaryotic_Translation_Initiation %R-DME-72613
RA_L13a-mediated_translational_ silencing_of_Ceruloplasmin_expression %R-DME-156827
-0.5 0.0 0.5
Encrichment Score (ES)
+Oleate vs Serum Starved DESeq2
KEGG_Fatty_acid_degradation%dme00071
KEGG_Propanoate_metabolism%dme00640
RA_Peroxisomal_protein_import %R-DME-9033241
KEGG_Peroxisome%dme04146
RA_Protein_localization %R-DME-9609507
RA_Transport_of_small_molecules% R-DME-382551
KEGG_Protein_processing_in_ endoplasmic_reticulum%dme04141
RA_Post-translational_protein_ phosphorylation%R-DME-8957275
RA_Regulation_of_Insulin-like_Growth_ Factor_(IGF)_transport_and_uptake_by_ IGFBPs%R-DME-381426
-log10(padj) *sign(ES)
3
2
1
0
-1
-2
-3
-0.5 0.0 0.5
Encrichment Score (ES)
+Oleate vs Serum Starved+3AT DESeq2
KEGG_Fatty_acid_degradation%dme00071
RA_Peroxisomal_protein_import %R-DME-9033241
RA_Protein_localization %R-DME-9609507
KEGG_Peroxisome%dme04146
RA_Transport_of_small_molecules% R-DME-382551
KEGG_Protein_processing_in_ endoplasmic_reticulum%dme04141
KEGG_Lysosome%dme04142
RA_Post-translational_protein_ phosphorylation%R-DME-8957275
RA_Regulation_of_Insulin-like_Growth_ Factor_(IGF)_transport_and_uptake_by_ IGFBPs%R-DME-381426
-0.5 0.0 0.5
Encrichment Score (ES)
Serum Starved+ 3AT vs Control DESeq2
RA_ROS_and_RNS_production_in_ phagocytes%R-DME-1222556
RA_Cellular_response_to_starvation %R-DME-9711097
KEGG_mTOR_signaling_pathway %dme04150
RA_Eukaryotic_Translation_Initiation %R-DME-72613
RA_SRP-dependent_cotranslational_ protein_targeting_to_membrane %R-DME-1799339
RA_Nonsense_Mediated_Decay_(NMD)_ independent_of_the_Exon_Junction_C omplex_(EJC)%R-DME-975956
RA_Cellular_response_to_heat_stress %R-DME-3371556
log10(padj) *sign(ES)
3
2
1
0
-1
-2
-3
-0.5 0.0 0.5
Encrichment Score (ES)

Fig. S2. Comparison of genes with significantly different ($p<0.05$, padj/FDR<0.1) mRNA levels in S2 cells cultured in Schneider's medium supplemented with FBS (Standard, STD) compared to those cultured medium supplemented with FBS and Oleic acid (+Oleate, OLE), unsupplemented medium (Serum Starved, STV), and unsupplemented medium with 3-amino-1,2,4-triazole (STVA). Differential gene expression was calculated DESeq2 (Love et al., 2014) at a significance of ($p <0.05$ and/or padj FDR<0.1). Complete DESeq2 generated differential gene lists for each condition are provided as supplemental spreadsheets Tables S1-S6.

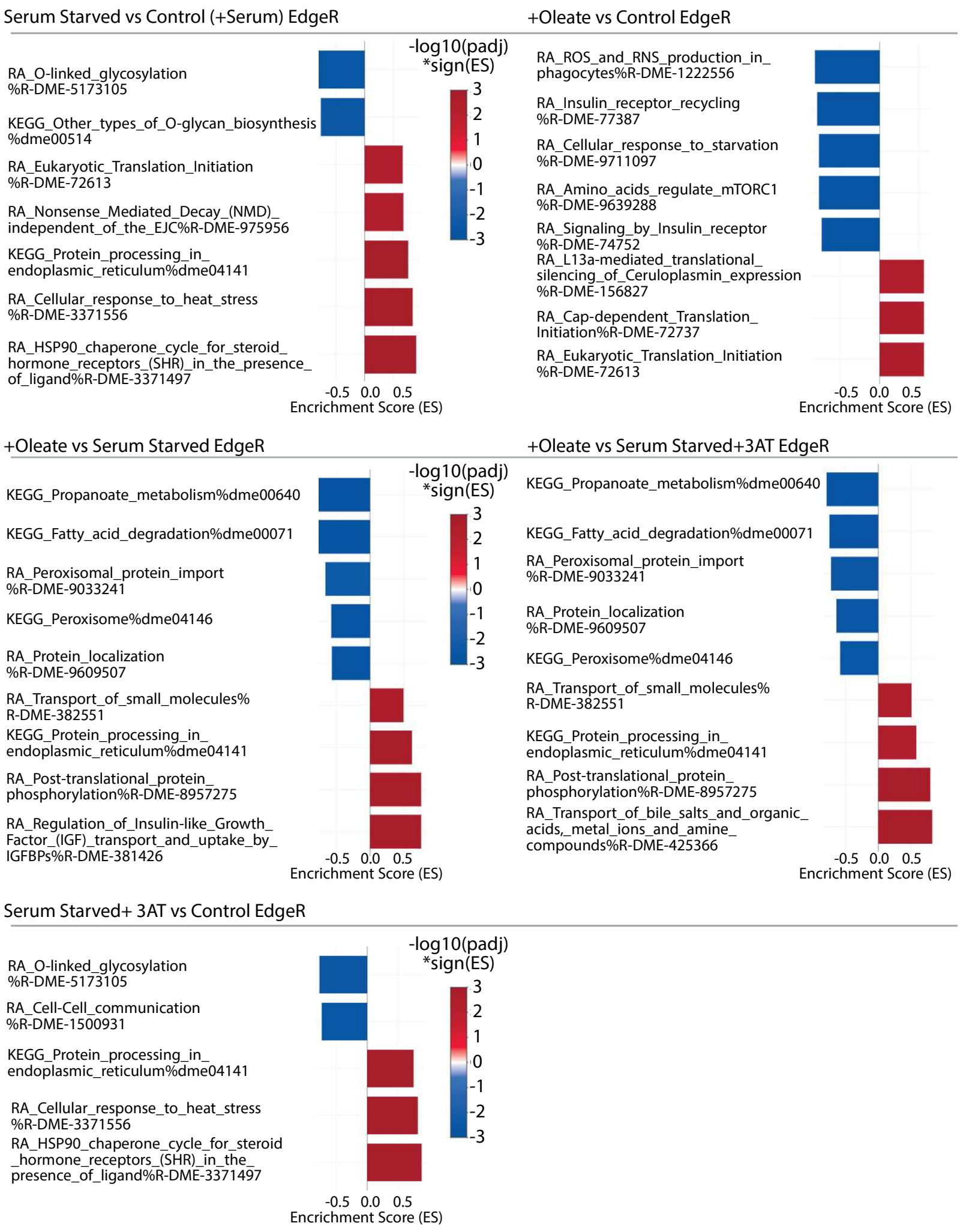

Fig. S3. Comparison of genes with significantly different ($p<0.05$, padj/FDR<0.1) mRNA levels in S2 cells cultured in Schneider's medium supplemented with FBS (Standard, STD) compared to those cultured medium supplemented with FBS and Oleic acid (+Oleate, OLE), unsupplemented medium (Serum Starved, STV), and unsupplemented medium with 3-amino-1,2,4-triazole (STVA). Differential gene expression was calculated EdgeR (Robinson et al., 2010) at a significance of ($p <0.05$ and/or padj FDR<0.1). Complete EdgeR generated differential gene lists for each condition are provided as supplemental spreadsheets Tables S1-S6.

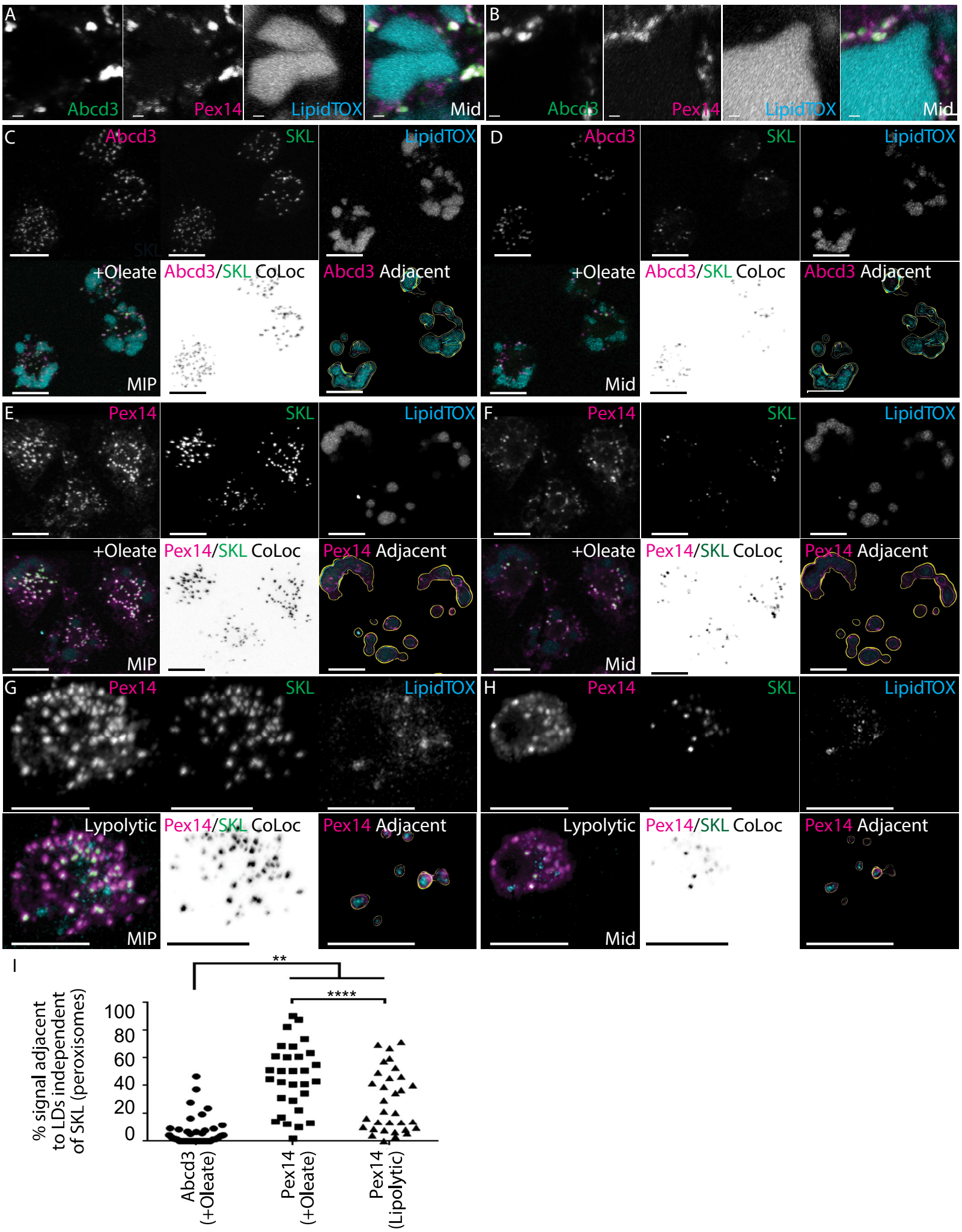

Supplementary Figure S4

Fig. S4. A-B) Much of the endogenous Pex14 concentrated in the regions surrounding LDs in fat body cells did not overlap mature peroxisomes (marked by endogenous Abcd3). C) Two independent markers of peroxisomes, punctate SKL (peroxisomal matrix) and the PMP Abcd3 transmembrane transporter largely co-localize (CoLoc) in S2 cells cultured in +Oleate conditions. A small proportion of the SKL/Abcd3 colocalized voxels are adjacent (lines indicate area 6 voxels from centroid mass) to LD interior (LipidTOX). A maximum projection (MIP) of an example 3-dimensional image used for co-localization is shown. D) A single confocal plane extracted from the three-dimensional image shown in C for illustration of image segmentation. All quantification was performed on the 3D volume. E) Comparison of Pex14, another peroxisomal PMP, with punctate SKL (peroxisomal matrix) in +Oleate cells. A larger proportion of the SKL/Pex14 colocalized voxels are adjacent (6 voxels from centroid mass) to LD interior (LipidTOX) in cultured in Lipolytic conditons. A maximum projection (MIP) of an example 3-dimensional image used for co-localization is shown. F) A single confocal plane from the image shown in E). G) Comparison of Pex14/SKL colocalized voxels are adjacent (6 voxels from centroid mass) to LD interior (LipidTOX). A maximum projection (MIP) of an example 3-dimensional image used for co-localization is shown. H) A single confocal plane from the image shown in E). Scale=2μm. I) There is a significant (** $p<0.01$) increase in Pex14 that is independent of other peroxisome markers compared to Abcd3 in cells cultured in either +Oleate and Lipolytic conditions. The amount of Pex14 adjacent to LDs independently of peroxisomes also drops significantly (**** $p<0.0001$) when cells are transferred from +Oleate to Lipolytic culture conditions.

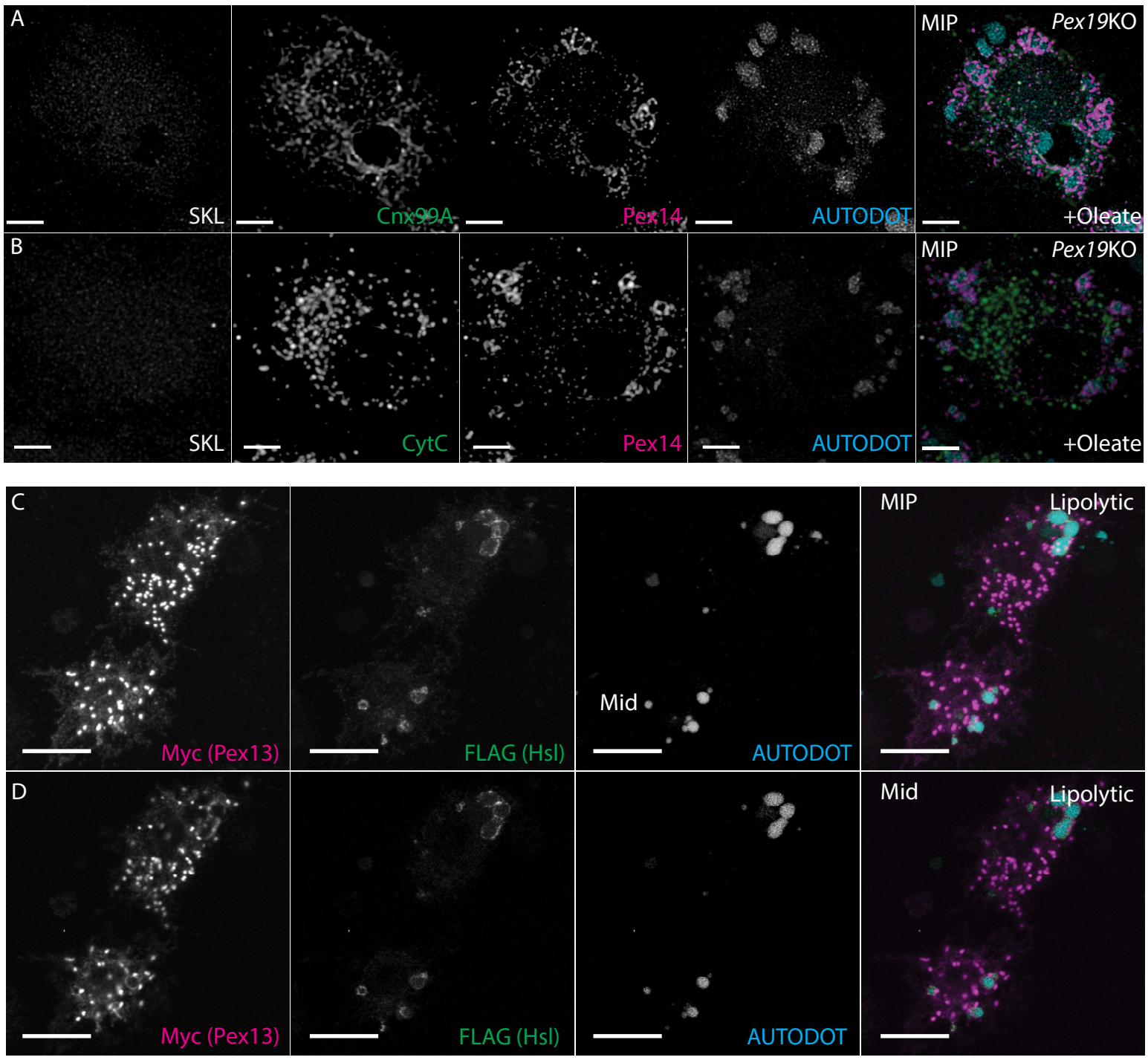

Fig. S5. A) Maximum intensity projection (MIP) images of *Pex19*KO S2R+ cell constitutively expressing mNeonGreen-SKL (peroxisome marker) are shown. No mature peroxisomes (SKL punctate) were observed. Endogenous Pex14 was observed surrounding LDs (AUTODOT) as does ER (Cnx99A). B) Maximum intensity projection (MIP) images show no appreciable co-localization between Pex14 surrounding LDs and a mitochondrial marker (CytC) throughout the three-dimensional cell volume. C) Co-overexpression of Hsl and Pex13 in Lipolytic condition suppressed LD fragmentation like Pex14. Unlike what is seen with Pex14 (Figure 5C-D), Hsl can be seen surrounding the same LDs as Pex13. C) A single confocal plane of the maximum projections. Scale=2µm.

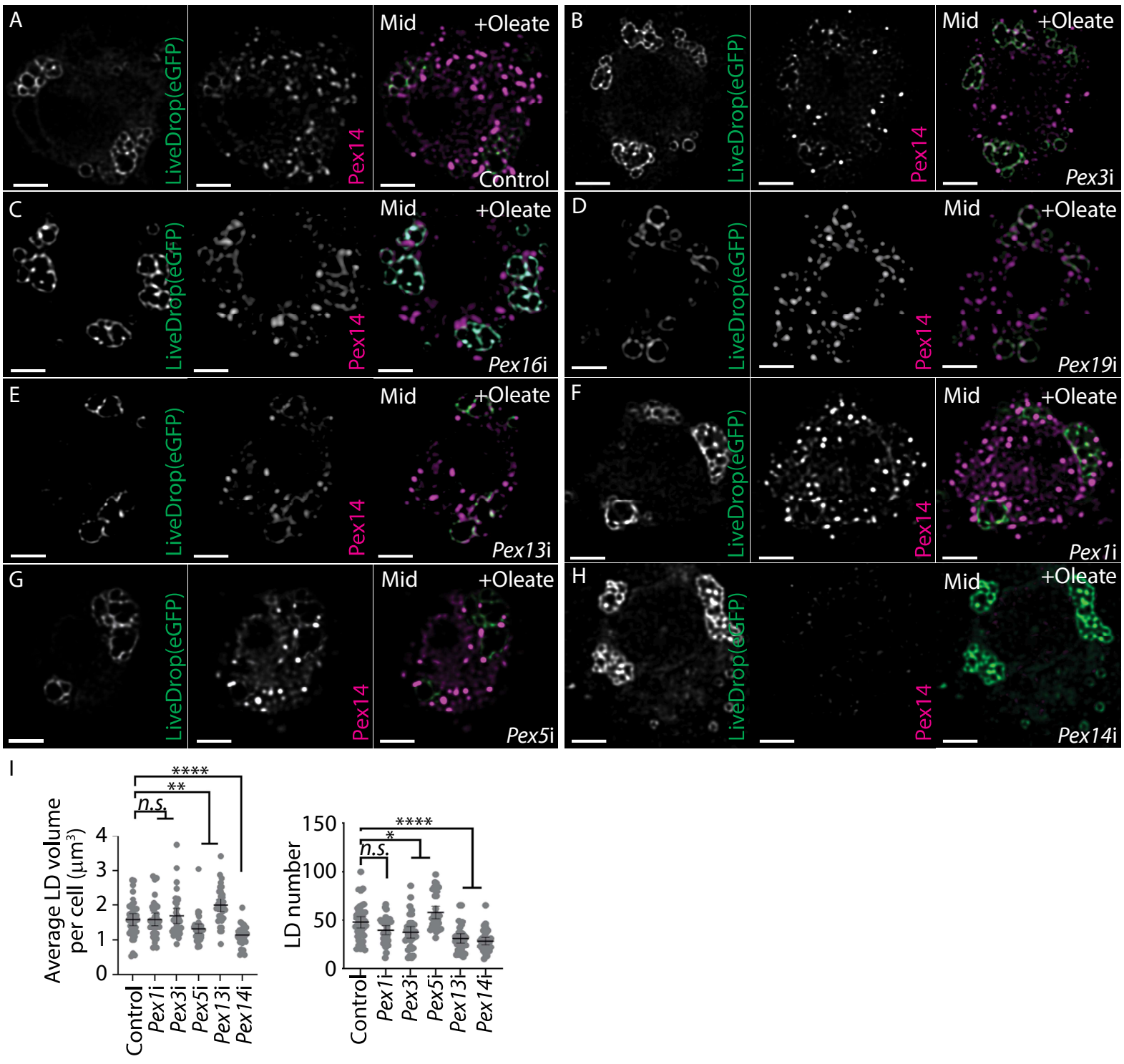

Fig. S6. Mid-volume single plane images corresponding to the MIP images and quantification of individual LD volume shown in Figure 7. Representative single confocal plane images of a *Drosophila* S2 cell stably expressing LiveDrop-GFP to mark the LD surface that was treated with *Pex*double-stranded RNA (*Pex*i). The scale bar represents 2µm. A) Control S2 cells had large, punctate peroxisomal dots while smaller, non-peroxisomal signals (left-center and bottom-right) co-localized with LiveDrop-GFP. B) *Pex3*i, C) *Pex16*i,D) *Pex19*i, and E) *Pex13*i treatment reduced Pex14 punctate and enhanced Pex14 co-localization with the LiveDrop marker of the LD surface. F) *Pex1*icells had smaller and relatively more peroxisomal Pex14 punctate spots and less Pex14 co-localization with LiveDrop. G) *Pex5*i cells all had relatively fewer punctate Pex14 spots compared to control cells but Pex14 enhancement to LDs was not observed. H) *Pex14*i cells had very little Pex14 signal. The LiveDrop signal in these cells outlined smaller and more numerous LD volumes. Scale=2µm. I) The number and average volume of LDs in *Pex*i cells overexpressing HA-Hsl.

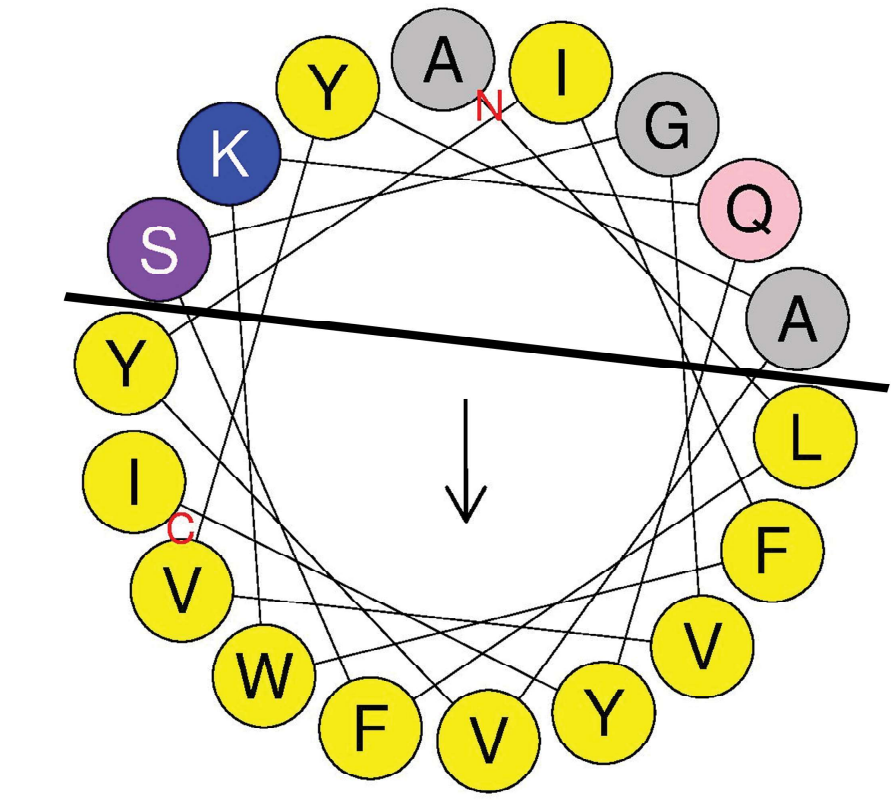

Fig. S7. A helical wheel projection of Pex14 between amino acids 124-141 within the TM domain generated by HeliQuest (Gautier et al., 2008). Amino acids within this region are shown as one letter code and the colored circles correspond to charged properties: Yellow (hydrophobic), purple and pink (polar), blue (charged), and grey (poorly hydrophobic). The dark line divides the hydrophobic and hydrophilic side of the amphipathic helix. The hydrophobic side consisting of 10 hydrophobic residues is predicted to be able to insert into the LD monolayer.

Table S1. STVvsCTL.xlsx - A curated list of differentially expressed genes identified ($p<0.05$) between STV-S2 cells cultured in Schneiders media with no supplement and CTL-S2 cells cultured in Schneiders media supplemented with FBS.

Click here to download Table S1

Table S2. OLEvsSTV.xlsx A curated list of differentially expressed genes identified ($p<0.05$) between OLE-S2 cells cultured in Schneiders media supplemented with 1μM oleic acid and STV-S2 cells cultured in Schneiders media no supplement.

Click here to download Table S2

Table S3. OLEvsCTL.xlsx A curated list of differentially expressed genes identified ($p<0.05$) between OLE-S2 cells cultured in Schneiders media supplemented with 1μM oleic acid and CTL-S2 cells cultured in Schneiders media supplemented with FBS.

Click here to download Table S3

Table S4. STVvsSTVA.xlsx A curated list of differentially expressed genes identified ($p<0.05$) between STV-S2 cells cultured in Schneiders media no supplement and STVA-S2 cells cultured in Schneiders media no supplement treated with 3-amino-1,2,4-triazole (3AT).

Click here to download Table S4

Table S5. STVAvsCTL.xlsx A curated list of differentially expressed genes identified ($p<0.05$) between STVA-S2 cells cultured in Schneiders media no supplement treated with 3-amino-1,2,4-triazole (3AT) and CTL-S2 cells cultured in Schneiders media supplemented with FBS.

Click here to download Table S5

Table S6. OLEvsSTVA.xlsx A curated list of differentially expressed genes identified ($p<0.05$) between OLE-S2 cells cultured in Schneiders media supplemented with 1μM oleic acid and STVA-S2 cells cultured in Schneiders media no supplement treated with 3-amino-1,2,4-triazole (3AT).

Click here to download Table S6